SOUTHERN PLAINS
TRANSPORTATION CENTER

Safety Evaluation of Pavement Surface Characteristics with 1mm 3D Laser Imaging

Kelvin C.P. Wang, Ph.D., P.E
Joshua Q. Li, Ph.D., P.E.

SPTC14.1-77-F

Southern Plains Transportation Center
201 Stephenson Parkway, Suite 4200
The University of Oklahoma
Norman, Oklahoma 73019

TECHNICAL REPORT DOCUMENTATION PAGE

1. REPORT NO.	2. GOVERNMENT ACCESSION NO.	3. RECIPIENTS CATALOG NO.
SPTC14.1-077		

4. TITLE AND SUBTITLE	5. REPORT DATE
Safety Evaluation of Pavement Surface Characteristics with 1mm 3D Laser Imaging	April 24, 2019
	6. PERFORMING ORGANIZATION CODE
7. AUTHOR(S)	8. PERFORMING ORGANIZATION REPORT
Kelvin C.P. Wang, Ph.D., P.E.; Joshua Q. Li, Ph.D., P.E.	Oklahoma State University
9. PERFORMING ORGANIZATION NAME AND ADDRESS	10. WORK UNIT NO.
School of Civil and Environmental Engineering Oklahoma State University Stillwater, OK 74078	11. CONTRACT OR GRANT NO. DTRT13-G-UTC36
12. SPONSORING AGENCY NAME AND ADDRESS	13. TYPE OF REPORT AND PERIOD COVERED
Southern Plains Transportation Center 201 Stephenson Pkwy, Suite 4200 The University of Oklahoma Norman, OK 73019	Final Oct 2014 – Dec 2016
	14. SPONSORING AGENCY CODE

15. SUPPLEMENTARY NOTES

University Transportation Center

16. ABSTRACT

This report documents the applications of 1mm 3D laser imaging technology to perform safety evaluation of pavements. Several state-of-the-art data collection devices were used for data collection, including the OSU 3D laser imaging technology (named as PaveVision3D Ultra) for 1mm 3D pavement surface data, the Inertial Measurement Unit (IMU), Grip Tester for continuous surface friction, dynamic friction tester (DFT) for dynamic friction coefficients, AMES high speed profiler for pavement roughness and macro-texture, and the portable LS-40 3D Surface Analyzer for ultra-high resolution pavement texture. The estimation of pavement cross slop, hydroplaning speed, macrotexture, and friction performance can be performed via the 3D pavement image at high resolution. This study with field pavement applications has shown that the 1mm 3D Ultra technology is promising in real-time pavement surface characterization and evaluation for both pavement and safety management at network and project level surveys. It is anticipated that more tests and refinements are to be performed to validate the new emerging 3D laser imaging technology as a single-pass and complete lane-coverage platform for multiple safety and pavement evaluation purposes.

17. KEY WORDS	18. DISTRIBUTION STATEMENT
Safety, 1mm 3D Laser Imaging, Hydroplaning, Macro-texture, Friction	No restrictions. This publication is available at www.sptc.org and from the NTIS.

19. SECURITY CLASSIF. (OF THIS REPORT)	20. SECURITY CLASSIF. (OF THIS PAGE)	21. NO. OF PAGES	22. PRICE
Unclassified	Unclassified	78	

Safety Evaluation of Pavement Surface Characteristics with 1mm 3D Laser Imaging

Final Report

SPTC14.1-077

April 2019

Kelvin C.P. Wang, Ph.D., P.E

Joshua Q. Li, Ph.D., P.E.

School of Civil and Environmental Engineering
Oklahoma State University
Stillwater, OK 74075

Southern Plains Transportation Center
OU Gallogy College of Engineering
201 Stephenson Pkwy, Suite 4200
Norman, OK 73019

APPROXIMATE CONVERSIONS TO SI UNITS

SYMBOL	WHEN YOU KNOW	MULTIPLY BY	TO FIND	SYMBOL
		LENGTH		
in	inches	25.4	millimeters	mm
ft	feet	0.305	meters	m
yd	yards	0.914	meters	m
mi	miles	1.61	kilometers	km
		AREA		
in^2	square inches	645.2	square millimeters	mm^2
ft^2	square feet	0.093	square meters	m^2
yd^2	square yard	0.836	square meters	m^2
ac	acres	0.405	hectares	ha
mi^2	square miles	2.59	square kilometers	km^2
		VOLUME		
fl oz	fluid ounces	29.57	milliliters	mL
gal	gallons	3.785	liters	L
ft^3	cubic feet	0.028	cubic meters	m^3
yd^3	cubic yards	0.765	cubic meters	m^3
		NOTE: volumes greater than 1000 L shall be shown in m^3		
		MASS		
oz	ounces	28.35	grams	g
lb	pounds	0.454	kilograms	kg
T	short tons (2000 lb)	0.907	megagrams (or "metric ton")	Mg (or "t")
		TEMPERATURE (exact degrees)		
^oF	Fahrenheit	5 (F-32)/9 or (F-32)/1.8	Celsius	^oC
		ILLUMINATION		
fc	foot-candles	10.76	lux	lx
fl	foot-Lamberts	3.426	$candela/m^2$	cd/m^2
		FORCE and PRESSURE or STRESS		
lbf	poundforce	4.45	newtons	N
lbf/in^2	poundforce per square inch	6.89	kilopascals	kPa

APPROXIMATE CONVERSIONS FROM SI UNITS

SYMBOL	WHEN YOU KNOW	MULTIPLY BY	TO FIND	SYMBOL
		LENGTH		
mm	millimeters	0.039	inches	in
m	meters	3.28	feet	ft
m	meters	1.09	yards	yd
km	kilometers	0.621	miles	mi
		AREA		
mm^2	square millimeters	0.0016	square inches	in^2
m^2	square meters	10.764	square feet	ft^2
m^2	square meters	1.195	square yards	yd^2
ha	hectares	2.47	acres	ac
km^2	square kilometers	0.386	square miles	mi^2
		VOLUME		
mL	milliliters	0.034	fluid ounces	fl oz
L	liters	0.264	gallons	gal
m^3	cubic meters	35.314	cubic feet	ft^3
m^3	cubic meters	1.307	cubic yards	yd^3
		MASS		
g	grams	0.035	ounces	oz
kg	kilograms	2.202	pounds	lb
Mg (or "t")	megagrams (or "metric ton")	1.103	short tons (2000 lb)	T
		TEMPERATURE (exact degrees)		
^oC	Celsius	1.8C+32	Fahrenheit	^oF
		ILLUMINATION		
lx	lux	0.0929	foot-candles	fc
cd/m^2	$candela/m^2$	0.2919	foot-Lamberts	fl
		FORCE and PRESSURE or STRESS		
N	newtons	0.225	poundforce	lbf
kPa	kilopascals	0.145	poundforce per square inch	lbf/in^2

*SI is the symbol for the International System of Units. Appropriate rounding should be made to comply with Section 4 of ASTM E380. (Revised March 2003)

Acknowledgements

This report was prepared under research project, “Safety Evaluation of Pavement Surface Characteristics with 1mm 3D Laser Imaging”, sponsored by the Southern Plains Transportation Center. The opinions expressed in the project are those of the authors, who are responsible for the accuracy of the facts and data herein, and do not necessarily reflect the official policies of the sponsoring agency. This report does not constitute a standard, regulation, or specification.

TABLE OF CONTENTS

1. INTRODUCTION 1

1.1 Background 1

1.2 Report Outline 2

2. HYDROPLANING ON SLOPING PAVEMENTS BASED ON INERTIAL MEASUREMENT UNIT (IMU) AND 1MM 3D LASER IMAGING DATA 4

2.1 Introduction 4

2.2 Prediction Models of Hydroplaning Speed 5

2.2.1 Gallaway and USF Models 5

2.2.2 Effects of Pavement Slope on Vertical Wheel Load 6

2.2.3 Improved Hydroplaning Speed Prediction Models 8

2.2.4 Sensitivity Analysis of the Improved Models 9

2.3 Data Acquisition Systems 10

2.3.1 Digital Highway Data Vehicle (DHDV) with PaveVision3D 10

2.3.2 Inertial Measurement Unit (IMU) 11

2.4 Data Preparation 11

2.4.1 Estimated Mean Texture Depth (EMTD) 11

2.4.2 Cross Slope Calibration 12

2.5 Automated Prediction Program of Hydroplaning 14

2.6 Case Study 15

2.6.1 Test Site 15

2.6.2 Selection of Sample Size 15

2.6.3 Local Rainfall Intensity 15

2.6.4 Cross Slope and Longitudinal Grade 15

2.6.5 EMTDs and WFDs 16
2.6.6 Hydroplaning Speed Estimation 17
2.6.7 Potential Hydroplaning Segment Detection 18
2.7 Conclusions 19
3. WAVELET BASED MACRO-TEXTURE ANALYSIS FOR PAVEMENT FRICTION PREDICTION 21
3.1 Introduction 21
3.1.1 Background 21
3.1.2 Objectives 22
3.2 Methodology 22
3.3 Data Collection and Preliminary Results 23
3.3.1 Data Collection 23
3.3.2 Preliminary Results 24
3.4 Wavelet Analysis of Macro-texture Profiles 27
3.4.1 Total Energy Analysis 28
3.4.2 Relative Energy Analysis 29
3.5 Friction Prediction Model 31
3.6 Conclusions 34
4. NOVEL MACRO- AND MICRO-TEXTURE INDICATORS FOR PAVEMENT FRICTION USING HIGH-RESOLUTION 3D SURFACE DATA 36
4.1 Introduction 36
4.1.1 Background 36
4.1.2 Objective 37
4.2 Field Data Collection 38

4.2.1 LTPP SPS-10 Testing Site 38
4.2.2 Data Collection Devices 40
4.3 Preliminary Results 41
4.4 3D Areal Texture Parameters 44
4.4.1 Height Parameters 44
4.4.2 Volume Parameters 45
4.4.3 Hybrid Parameters 46
4.4.4 Spatial Parameters 47
4.4.5 Feature Parameters 47
4.5 Selection of 3D Texture Parameters 48
4.5.1 Correlation Analysis 48
4.5.2 Correlation within Each Category 48
4.5.3 Correlation among Categories 49
4.6 Friction Prediction Model based on selected 3D Areal Texture Parameters 52
4.6.1 Model Development 52
4.6.2 Model Verification 53
4.7 Conclusions 56
5. CONCLUSIONS 58
REFERENCES 61

List of Figures

Figure 1 Diagram of Cross Slope, Longitudinal Grade, and Flow Path 6

Figure 2 Vehicle on Segment with (a) Longitudinal Grade; (b) Horizontal Curve 8

Figure 3 Sensitivity of Hydroplaning Speed (a) Longitudinal Grade; (b) Cross Slope ... 10

Figure 4 DHDV Vehicle (a) Exterior Appearance; (b) Working Principle 11

Figure 5 Example 3D (right) and 2D (left) Surface Data (courtesy of WayLink) 11

Figure 6 Cross Slope Calibration Using IMU and 3D Laser Imaging Data 14

Figure 7 AHPP Software Interface 14

Figure 8 Geometry of Test Site: (a) Longitudinal Grade; (b) Cross Slope 16

Figure 9 WFDs and EMTDs of Test Site: (a) WFDs; (b) EMTDS. 17

Figure 10 Hydroplaning Test Site: (a) Hydroplaning Speed; (b) Hazardous Segments 19

Figure 11 Example Site with Distinct Friction and MPD (Data Collection #7) 25

Figure 12 – Example Site with Distinct Friction Only (Data Collection #1) 26

Figure 13 Scatter Plot of Friction Number and MPD (Data Collection #1) 27

Figure 14 Wavelet Decompositions of Macro-texture Profiles 28

Figure 15 Energy Distribution 29

Figure 16 Cumulative Relative Energy Distribution 30

Figure 17 Pavement Friction Prediction Results 33

Figure 18 LTPP SPS-10 Site in Oklahoma 39

Figure 19 Data Collection Devices and Example Data Sets 40

Figure 20 Average DFT Friction at Various Speeds and Summary of MPD 42

Figure 21 Calculation of Volume Parameters 46

Figure 22 Comparisons of Selected 3D Pavement Texture Parameters 51

Figure 23 Model Validation and Comparisons..... 55

List of Tables

Table 2.1 Average Precipitation in Spavinaw Station (23)..... 15

Table 2.2 Samples of 3D Imaging Data and IMU Data for Hydroplaning Speed Calculation 18

Table 3.1 HFST Sites for Data Collection..... 24

Table 3.2 Correlation Coefficients between RE and Friction Number 30

Table 3.3 Estimated Coefficients and P-value for Friction Prediction Model 31

Table 3.4 Statistic Result of Comparison between Measured and Predicted Friction Number 32

Table 4.1 Experiment Design for LTPP SPS-10 Site in Oklahoma 38

Table 4.2 Correlation Analyses of 3D Height Texture Parameters..... 49

Table 4.3 Correlation Analyses of 3D Volume and Hybrid Texture Parameters..... 50

Table 4.4 Correlation Analyses of 3D Spatial and Feature Texture Parameters..... 50

Table 4.5 Correlation Analyses Among All Categories of 3D Texture Parameters..... 50

Table 4.6 Significance of Selected 3D Texture Parameters on DFT Friction at Different Speeds..... 52

Table 4.7 Statistic Results of Friction Prediction Models based on Selected 3D Areal Texture Parameters 53

Table 4.8 Statistic Results of Friction Prediction Models based on MPD 53

1. INTRODUCTION

1.1 Background

It has been shown that approximately one quarter of highway fatalities in the United States occur at or near horizontal curves (http://www.highfrictionroads.com/). Contributing factors to these run-off-the-road crashes include excessive vehicle speed, distracted driving, and driver error. At some locations, the deterioration of pavement surface friction may also be a factor, particularly during wet weather. In an effort to reduce the deaths and injuries that occur along these horizontal curves, the Federal Highway Administration Office of Pavement Technology has initiated the Surface Enhancements At Horizontal Curves (SEAHC) program for the installation and demonstration of friction enhancing treatments at numerous horizontal curves to isolate and demonstrate the effects of increasing surface friction on the number of accidents at these select locations. Therefore, collecting pavement safety data is a critical process to start analysis and research on safety characteristics based on pavement surface.

Data collection on pavement surfaces includes longitudinal profile for roughness, transverse profile for rutting, macro-texture and friction for safety, and cracking and various other surface defects for distresses. Pavement data collection technologies have improved gradually in the last few decades, particularly for profiling. However, due to sensor and computing limitations and inadequate research funding, the hardware and software necessary to automatically obtain pavement safety data based on surface characteristics is limited to using separate traditional instruments only capable of measuring characteristics on small areas on pavements. For instance high-speed friction tester of various types and macro-texture sensors can only collect data on a line on pavement; while high-precision friction and texture measurement instruments are usually static, time-consuming, and can only cover very small area on pavements. In addition, high-speed line-of-sight or point laser sensors for macro-texture measurement is based on decades' old design and electronics, and need substantial noise filtering to obtain signal data that is no longer as high-fidelity and high-resolution as needed for analysis.

Starting in the mid-1990's, the Arkansas State Highway and Transportation Department (AHTD), the Oklahoma Department of Transportation (ODOT), the US DOT University Transportation Centers (UTC) program, and the National Cooperative Highway Research Program (NCHRP) program, FHWA, and FAA provided funding support to the team led by the PI on various technology developments on pavement information systems and automated condition survey. The most significant development occurred in the last five years during which the team developed and implemented a 3D laser imaging sensor for pavement condition survey called PaveVision3D. Around 2011, the research team reached another milestone and completed the development of the PaveVision3D Ultra (3D Ultra). The 3D Ultra system can scan the pavement surface at true 1mm resolution in all three dimensions at the data collection speed of 60 MPH. The performance of the 3D Ultra is unprecedented and unparalleled. Technologies based on 3D Ultra are implemented or used by FHWA, FAA, Arkansas DOT, Oklahoma DOT, and several international users.

The measurement of pavement surface characteristics for safety analysis can be a direct application of 3D laser images as the 3D data can represent actual or virtual pavement surfaces with full-lane coverage. In particular, the new 3D Ultra technology is capable of gathering true 1mm resolution 3D data in all three dimensions at highway speed. Pavement surface data gathered at this speed and resolution provide engineers advantages in cost, visualization and analysis for safety concerns. As a matter of fact, the vertical resolution is about 0.3mm with the 3D Ultra system, where 1mm is represented with 3 vertical pixels or data points.

Therefore, with 3D image data representing actual pavement surface at full-lane coverage, it is possible to create a true representation of pavement surface at 1mm resolution which in turn can be used as input data for pavement safety analysis. The primary objectives of the proposed research are (1) to establish geographically and geometrically true pavement surface at 1mm resolution with a high-precision Inertial Measurement Unit (IMU), (2) to determine cross-slop, pavement edge falloff, and roadway geometric data for safety analysis, and (3) to automatically evaluate full-lane pavement macro-texture, and hydroplaning potential.

1.2 Report Outline

This report is presented with applications of 1mm 3D laser imaging technology to perform safety evaluation of pavements. Several state-of-the-art data collection devices were used for data collection, including the OSU 3D laser imaging technology (named as PaveVision3D Ultra) for 1mm 3D pavement surface data, the Inertial Measurement Unit (IMU), Grip Tester for continuous surface friction, dynamic friction tester (DFT) for dynamic friction coefficients, AMES high speed profiler for pavement roughness and macro-texture, and the portable LS-40 3D Surface Analyzer for ultra-high resolution pavement texture. Pavement surface characteristics in this report include pavement estimated hydroplaning speed, surface texture from AMES and LS-40, and friction from Grip Tester and DFT.

In Chapter 2, the IMU data and 3D laser imaging data are combined together to realistically model vehicle movements on cross slopes. The case study demonstrates the improved models are able to provide reasonable hydroplaning speed estimation based on 1mm 3D image to perform pavement safety evaluation in hydroplaning perspective. In Chapter 3, pavement macro-texture data from different pavement surfaces are analyzed via wavelet methodology to explore their contribution in friction performance at multi-level. Chapter 4 applies novel texture parameters at macro- and micro- level on high resolution pavement 3D image to capture pavement texture as well as friction characteristics simultaneously. The result indicates it is feasible to predict pavement friction number according to pavement texture characteristics to better address pavement safety performance in friction.

2. HYDROPLANING ON SLOPING PAVEMENTS BASED ON INERTIAL MEASUREMENT UNIT (IMU) AND 1MM 3D LASER IMAGING DATA

2.1 Introduction

Pavement hydroplaning occurs when water pressures build up in front of a moving tire resulting in an uplift force sufficient to separate the tire from the pavement. The loss of steering and traction force produced during hydroplaning may cause the vehicle to lose control, especially when a steering tire is involved (1). Past studies indicated the occurrence of hydroplaning is highly associated with several factors, including pavement texture, cross slope, longitudinal grade, pavement width, pavement types, pavement condition, tire characteristics, and rainfall intensity (2 and 3).

Numerous field studies were dedicated to developing hydroplaning prediction models in the past decades (4). The models can be grouped into two categories: empirical models and analytical models (5). The empirical methods use experimental data and equations to predict hydroplaning, including Road Research Laboratory (RRL) equations to estimate water film depth (WFD) (6), National Aeronautics and Space Administration (NASA) models developed based on aircraft tire and airport pavement data (4), and Gallaway model to predict roadway hydroplaning (7). The analytical methods attempt to mathematically model hydroplaning of the sheet flow and its interaction with a tire, including PAVDRN computer program developed by Pennsylvania State University (8), and the University of South Florida (USF) model based on Ong and Fwa's numerical prediction (9).

Pavement slope, also termed as flow path slope, consists of cross slope and longitudinal grade, which exerts a tremendous influence on hydroplaning prediction (10). To maintain constant water film, hydroplaning simulation tests in past studies were conducted on straight and flat pavements (11 and 12). For pavement segments with horizontal curve and large longitudinal grade, a smaller uplift force of water can cause hydroplaning issues due to the reduced vertical wheel load caused by large slopes. However, past studies on hydroplaning prediction neglected the influences of pavement slope on vertical wheel loads of vehicles. The existing hydroplaning prediction models overestimate hydroplaning speed, and are particularly not suitable to analyze pavements with large pavement slope.

The aims of this study include: 1) properly predict hydroplaning speeds on pavement with large slopes using hydroplaning prediction model; 2) calibrate the IMU measured cross slope by eliminating the effects of survey vehicle vibration; 3) identify the potential hydroplaning segments in network level survey. In order to achieve these aims, first, two improved models are presented in this study on the basis of the existing Gallaway and USF models, in which the effects of flow path slope on vertical wheel load are considered and the sensitivities of the variables to hydroplaning speed predictions are examined. In this study, the WayLink Digital Highway Data Vehicle (DHDV) with the new 1mm 3D PaveVision3D Ultra technology and an Inertial Measurement Unit (IMU) system is used to collect pavement surface data including 1mm 3D laser imaging data, cross slope, and longitudinal grade data. The 1mm 3D pavement surface data is directly used for estimating pavement macro-texture in lieu of using traditional spot-laser devices. Texture data is a key input for the presented hydroplaning models. A flexible pavement section with five horizontal curves is chosen as examples to investigate the potential hydroplaning risks of both straight roads and curved roads. Finally, based on the predicted hydroplaning speed and posted speed limit, pavement segments with potential hydroplaning risk can be identified for pavement engineers to take corrective measures such as constructing superior texture, posting proper speed traffic signs etc. to minimize potential traffic accidents caused by hydroplaning issues, and enhance pavement safety.

2.2 Prediction Models of Hydroplaning Speed

2.2.1 Gallaway and USF Models

The Gallaway model is an empirical method developed by Gallaway et al. (1979) for the US Department of Transportation. The method described in Equation 2.1-2.5 was adopted in the Texas Department of Transportation Hydraulic Design Manual (7). The flow path, an important factor on hydroplaning prediction model, can be defined in Figure 1 and calculated with Equation 2.1. The USF model is an analytical hydroplaning prediction model developed at the University of South Florida based on Ong and Fwa's comprehensive numerical prediction, shown in Equation 2.6. The USF model can be used to predict the hydroplaning speeds for different light vehicles that employ tires compatible with the locked-wheel tester tires (9).

$$S_f = SQRT(S_l^2+S_c^2) \quad (2.1)$$

$$L_f = W_p \times (S_f / S_c) \quad (2.2)$$

$$WFD = 0.01485 \times [(MTD^{0.11} \times L_f^{0.43} \times I^{0.59})/(S_c^{0.42})] - MTD \quad (2.3)$$

$$A = Max.\{[(12.639/WFD^{0.06})+3.50], [(22.351/WFD^{0.06})-4.97] \times MTD^{0.14}\} \quad (2.4)$$

$$v_p = 0.9143 \times SD^{0.04} \times P_t^{0.3} \times (TD+0.794)^{0.06}) \times A \quad (2.5)$$

$$v_p = W^{0.2} \times P_t^{0.5} \times [(0.82/WFD^{0.06})+0.49] \quad (2.6)$$

Where, WFD: Water film depth (mm); MTD: Mean texture depth (mm) calculated from the macro texture data; v_p: Hydroplaning speed (km/h); L_f: Pavement flow path length (m); S_c: Cross slope (m/m); S_l: Longitudinal grade (m/m); W_p: Pavement width (m); I: Rainfall intensity (mm/h); P_t: Inflation pressure (Kpa); SD: Spin down ratio; TD: Tire tread depth (mm); W: Wheel load (N).

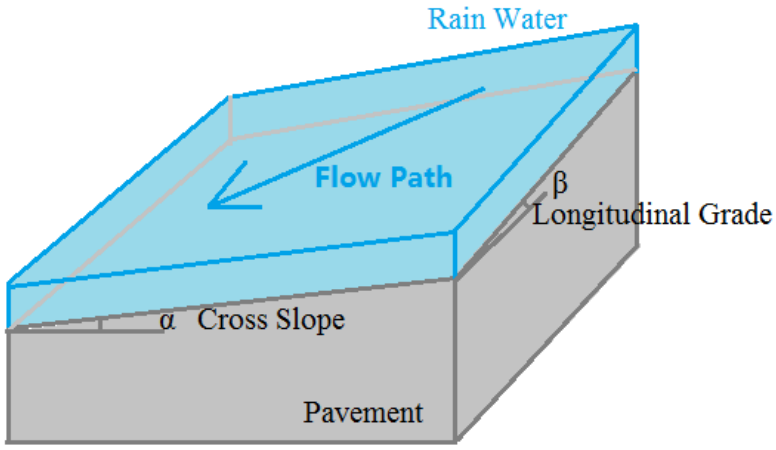

Figure 1 Diagram of Cross Slope, Longitudinal Grade, and Flow Path

2.2.2 Effects of Pavement Slope on Vertical Wheel Load

Typically cross slope or longitudinal grade would reduce the vertical wheel load of vehicles on pavement surface (13). Hydroplaning occurs when the vertical wheel load is equivalent to the uplift force by water (Equation 2.7), and the steering and traction force would be lost during hydroplaning.

Figure 2 (a) shows the pavement section with a large longitudinal grade. When the vehicle travels on this pavement segment, the vehicle gravity center would be partitioned into two components of forces: one (wheel load) is perpendicular with the travelling surface, and the other one (traction force) is parallel with pavement surface.

The wheel load would decrease with the increase of longitudinal grade (Equation 2.8), and the reduced wheel load would increase the hydroplaning risk.

Figure 2 (b) shows the pavement section with horizontal curves or large cross slope. Similarly, the vehicle gravity center is partitioned into two components of forces when the vehicle travels on the horizontal curve. One component of force is the wheel load, and the other one is the centripetal force shown in Figure 2 (b). The wheel load on horizontal curve would decrease with the increase of super-elevation (Equation 2.9). Finally the wheel load can be calculated with flow path slope by combining the cross slope and longitudinal grade, as given in Equation 2.10.

$$F_{UP} = W \quad (2.7)$$

$$W_L = G \times \cos(\beta) \quad (2.8)$$

$$W_C = G \times \cos(\alpha) \quad (2.9)$$

$$W = G \times \cos(\rho) \quad (2.10)$$

Where: F_{UP} - Minimum uplift force causing hydroplaning (N); W -- Wheel load (N); W_L - Wheel load in longitudinal section (N); W_C - Wheel load in cross section (N); G - Gravity of vehicle (N); β - Angle of longitudinal grade (degree); α-- Angle of cross slope (degree); ρ -- Angle of flow path slope (degree).

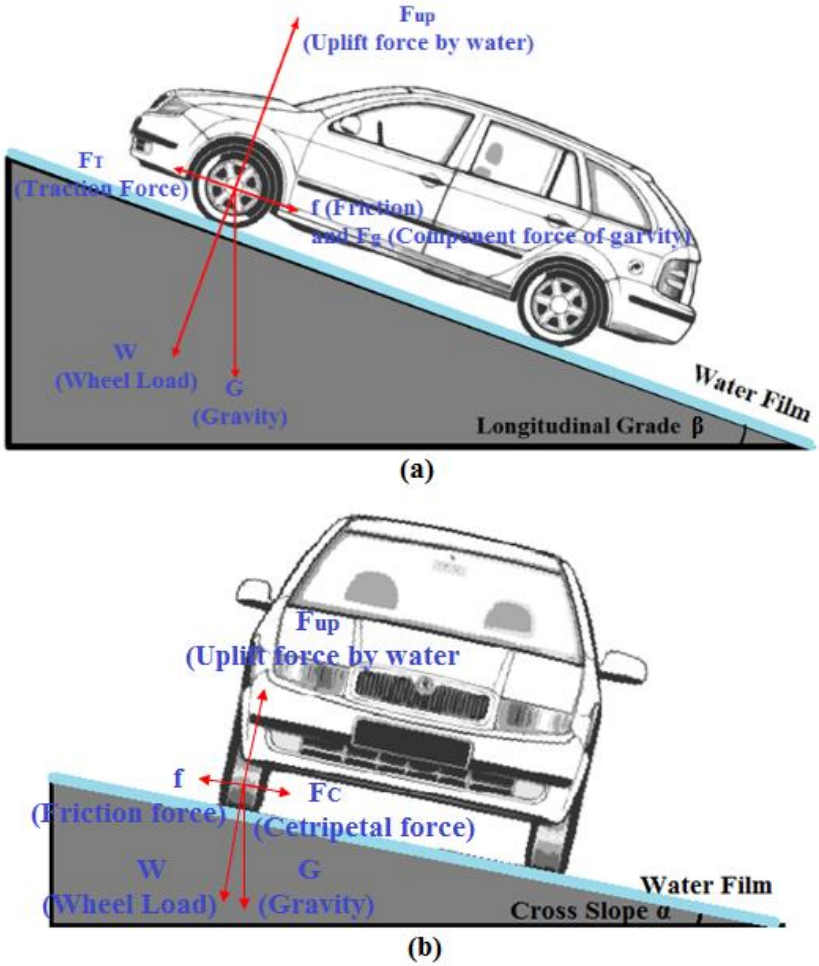

Figure 2 Vehicle on Segment with (a) Longitudinal Grade; (b) Horizontal Curve

2.2.3 Improved Hydroplaning Speed Prediction Models

In the current models, the influences of flow path slope on vertical wheel load are not taken into account in hydroplaning prediction models. Therefore this study aims at improving the existing Gallaway and USF models by considering the effects of flow path slope on wheel loads, as shown in Equations 2.11 and 2.12.

$$v_p = 0.9143 \times SD^{0.04} \times (P_t \times \cos\rho)^{0.3} \times (TD+0.794)^{0.06}) \times A \quad (2.11)$$

$$v_p = (W \times \cos\rho)^{0.2} \times (P_t \times \cos\rho)^{0.5} \times (0.82/WFD^{0.06} + 0.49) \quad (2.12)$$

Where: W - Wheel load (N); WFD - Water film depth (mm); P_t - Inflation pressure (Kpa); SD - Spin down ratio; TD - Tire tread depth (mm); A -- Maximum value of Equation (2.4); ρ - Angle of flow path slope (degree).

2.2.4 Sensitivity Analysis of the Improved Models

To explore the sensitivity of cross slope and longitudinal grade on hydroplaning speed, the cross slope and longitudinal grade change by ± 25%, ± 50%, and ± 75% individually while the other variables are maintained constant values. The constant values of each factor is assumed to be the average values of that factor measured for test site, as provided as follows:

- Cross slope: S_c = 1.53%,
- Rainfall intensity: I =148.4 mm/hr,
- Mean texture depth: MTD = 1.2mm,
- Longitudinal grade: S_1 = 1.32%.

The results of sensitivity analysis from the improved Gallaway and USF models to cross slope and longitudinal grade are given in Figure 3. It can be seen that the resulting change in hydroplaning speed, "VP", is apparent along the increase of cross slope and longitudinal grade. In the two improved models, the hydroplaning speed is affected by both the vertical load and the flow path length. Typically the increase in cross slope or longitudinal grade would diminish the vertical wheel load. The increase in cross slope would shorten the flow path length, while the increase in longitudinal grades would extend the flow path length. Both the decrease in vertical load and the increase in flow path length would reduce the hydroplaning speed.

Accordingly the hydroplaning speed should decrease with the increase of longitudinal slope, and may either increase or decrease with the increase of cross slope depending on effects of vertical load and flow paths. Figure 3 shows that hydroplaning speed goes up with the increase of the cross slope, indicating the effect of flow path length on hydroplaning speed is greater than that of wheel load. It is shown that hydroplaning speed is more sensitive to the cross slope than longitudinal grade in the two improved models.

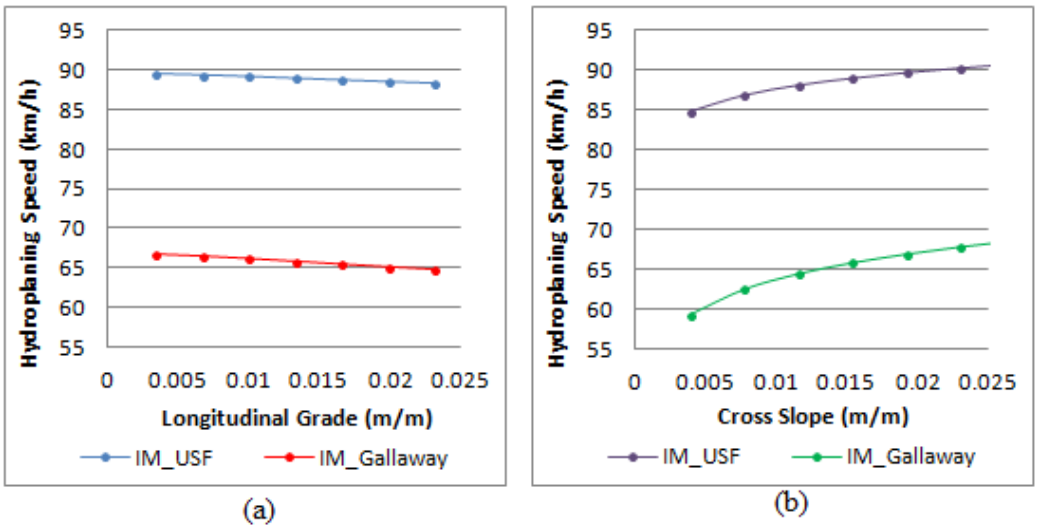

Figure 3 Sensitivity of Hydroplaning Speed (a) Longitudinal Grade; (b) Cross Slope

2.3 Data Acquisition Systems

2.3.1 Digital Highway Data Vehicle (DHDV) with PaveVision3D

DHDV, developed by the WayLink Systems Corporation with collaborations from the University of Arkansas and the Oklahoma State University, has evolved into a sophisticated system to conduct full lane data collection in 3D on roadways at highway speed up to 100 km/h. With the latest PaveVision3D Ultra (3D Ultra in short), the resolutions of surface 3D data are about 0.3 mm in vertical direction and 1 mm in the longitudinal and transverse directions, all achieved at 100km/h data collection speed. Figure 4(a) shows the exterior of a DHDV equipped with the 3D Ultra technology. With the high power line laser projection system and custom optic filters, DHDV can work at highway speed during day-time and night-time and maintain image quality and consistency. 3D Ultra is the latest imaging sensor technology that is able to acquire both 2D and 3D laser imaging data from pavement surface through two separate left and right sensors (14). The camera and laser working principle is shown in Figure 4(b). A typical pavement surface in 3D captured at highway speed is shown in Figure 5 with cracking analysis result.

Figure 4 DHDV Vehicle (a) Exterior Appearance; (b) Working Principle

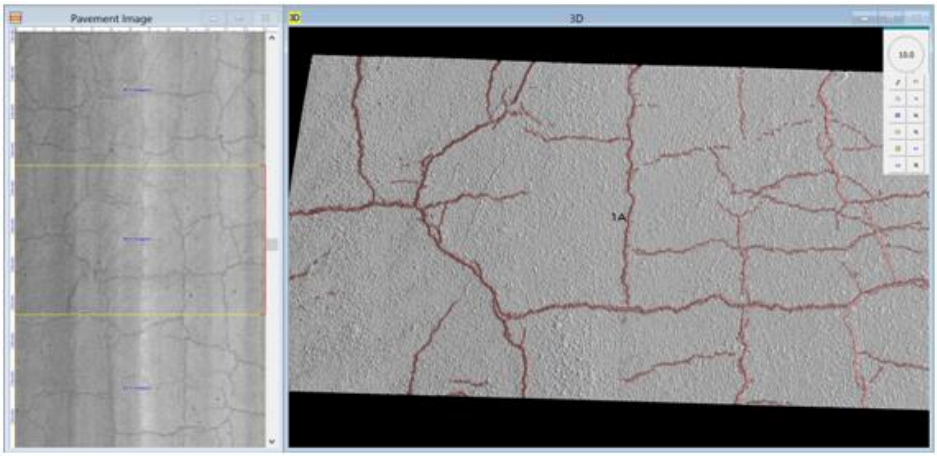

Figure 5 Example 3D (right) and 2D (left) Surface Data (courtesy of WayLink)

2.3.2 Inertial Measurement Unit (IMU)

The Inertial Measurement Unit (IMU) used for 3D Ultra is a self-contained sensor consisting of accelerometers, fiber-optic gyroscopes, and integrated GPS antennas. The physical principle of this type of gyroscope operation is analogous to the Doppler Effect, which involves determination of the phase shift between two counter propagating light beams (15). Currently the IMU has been integrated and synchronized into the DHDV vehicle for geometrical information capture. In this study the collected IMU data contains GPS coordinates, cross slope, and longitudinal grade, which are utilized for hydroplaning speed prediction.

2.4 Data Preparation

2.4.1 Estimated Mean Texture Depth (EMTD)

The methodologies for texture measurements can be grouped into two categories: static and high-speed methods. The static test methods include Sand Patch

Method (16), Circular Track Meter (17), and Outflow Meter (18), and their measurements are conducted on the marked or specified small areas. The traditional high-speed test techniques are characterized with the laser based data acquisition systems (19) with a spot laser resulting in a single line of measurement along the longitudinal direction of pavement. The measurements are continuously conducted on test sections, which can be regarded as an efficient tool for network level pavement survey.

The widely used texture indicators include the Mean Profile Depth (MPD) and Mean Texture Depth (MTD) (16 and 20). In this study the MTD methodology is applied since the estimation of water film depth is dependent on the MTD in the hydroplaning models. However, as the manual process to obtain MTD through the Sand Patch Method is a standard, time-consuming, and somewhat not reliable enough (21), the 3D pavement surface captured with the 3D Ultra technology is therefore used as an alternative to be used as input to calculate area texture simulating the Sand Patch Method. The alternative substantially improves data collection efficiency and reliability of computing surface texture. As a volumetric method, the Estimated MTD (EMTD) is therefore introduced in the research by simulating the Sand Patch Method with 1mm 3D laser imaging data of the entire lane, as shown in Equation 2.13 (22). EMTD and MTD are assumed to be equivalent in the presented research.

$$EMTD = (1/k) \times Sum_k\{Sum_x[Sum_y(F_0-F(x,y))]/D\} \quad (2.13)$$

Where: Sum_k is the summation in terms of k, F(x,y) – The pixel depth at point (x, y); D – The integral or gridded area containing of M×N pixels; F_0 – The maximum peak in each area D; k – The number of grids within the test sample.

2.4.2 Cross Slope Calibration

A properly designed and constructed cross slope is important for safe travelling since inadequate cross slopes may result in low efficiency in drainage and large cross slopes may lead to vehicle manoeuvring difficulties. Therefore, the accurate measurement of cross slope is important for hydroplaning speed prediction. In this study, 1mm 3D pavement data and IMU data are combined together to reproduce the cross slope of pavements.

IMU mounted on the vehicle can measure three Euler angles, which are termed as roll (Euler angle about x-axis), pitch (Euler angle about y-axis) and yaw (Euler angle about z-axis) respectively. The roll angle is to represent pavement cross slope, and pitch angle is traditionally used to represent pavement longitudinal grade based on the assumption that the vehicle floor is parallel with pavement surface during travelling. However, in real world the vehicle floor is not parallel with pavement surface during travelling, which can be caused by: 1) uneven gravity distribution of the vehicle; 2) vibration of the vehicle during travelling; 3) pavement surface geometry and condition.

This study attempts to measure the vehicle's body roll angle in X coordinate (angle γ) using the collected 3D laser imaging data. Two sensors mounted on the rear of the DHDV are capable of covering the entire lane. The “true” cross slope of pavements can be approximately determined with two parameters: the tilt of the vehicle floor and the slope of pavement surface captured by 3D cameras (23). As Figure 6 shows, the IMU system measures the angle θ of the vehicle relative to a level datum. γ is the vehicle vibration angle in X coordinate which can be calculated in Equation 2.14. The "true" cross slope can be obtained by Equation 2.15. However, in real world the angle and are very small, so the cross slope can be directly computed as the difference in slope of θ and slope of γ (Equation 2.16) (24).

$$\gamma = \text{act}\tan[(y_2-y_1)/L] \quad (2.14)$$

$$\alpha = \tan(\theta+\gamma) \quad (2.15)$$

$$\alpha = \tan(\theta)+ \tan(\gamma) \quad (2.16)$$

Where: α – Angle of cross slope (degree); γ – The body roll angle of vehicle (degree); θ – IMU roll angle (degree); L – The distance between left and right laser (m); y_1 – The vertical distance from left sensor to the pavement surface (m); y_2 – The vertical distance from right sensor to the pavement surface (m).

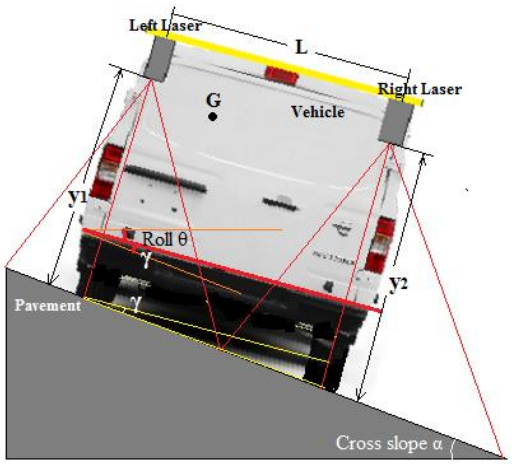

Figure 6 Cross Slope Calibration Using IMU and 3D Laser Imaging Data

2.5 Automated Prediction Program of Hydroplaning

A software program named Automated Hydroplaning Prediction Program (AHPP) is developed in this study to implement data processing and analysis. Figure 7 shows the main interface of AHPP. Once users import the IMU and 3D image data into AHPP, the two types of data (1mm 3D laser imaging data and IMU data) can be automatically matched by Distance Measurement Instrument (DMI) pulses, and the calibrated cross slope can be produced by the integration of IMU data and 3D data. In AHPP, users can manually assign the local rainfall intensity and pavement types. The AHPP outputs include EMTD, WFD, calibrated cross slope, longitudinal grade, and predicted hydroplaning speeds from various models.

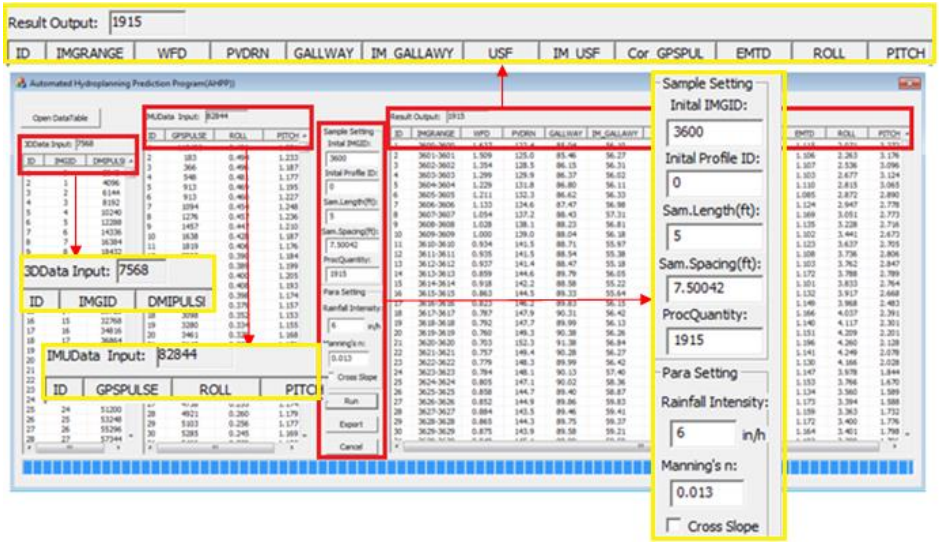

Figure 7 AHPP Software Interface

2.6 Case Study

2.6.1 Test Site

A flexible pavement section located in Spavinaw, Oklahoma is chosen as the test section, which starts from the location (Latitude: 36.329175, Longitude: -95.081696), and ends with the location (Latitude: 36.351066, Longitude: -95.062796), with a length of 4.35 km. The pavement of the test lane is in excellent condition and has a width of 3.65m. On this test section there are five horizontal curves.

2.6.2 Selection of Sample Size

The 3D laser imaging data collected with the 3D Ultra DHDV is stored on computer hard disk in the form of raw data files with the size of 4096 pixel wide by 2048 pixel long. The raw data files are used as basic input data sets, or samples, and subsequently data processing and analysis are conducted on each individual sample. In this study one raw image is considered as a sample (2.28m long) and the entire pavement section consists of 1915 samples.

2.6.3 Local Rainfall Intensity

The local rainfall intensity at the test site is obtained from National Oceanic and Atmospheric Administration's (NOAA) National Water Service database (25). Table 2.1 shows the precipitation in Spavinaw Station Oklahoma from NOAA database. The two-year return period storm with duration of five minutes is used in Gallaway and USF models for rainfall intensity acquisition. Based on NOAA database, the rainfall intensity of 148.4mm/hour is used for the test site.

Table 2.1 Average Precipitation in Spavinaw Station (23)

Duration (in mm)	1-Year	2-Year	5-Year	10-Year
5 min	10.87	12.37	14.91	17.04
10 min	15.93	18.11	21.82	24.97
15 min	19.41	22.09	26.67	30.48
30 min	28.70	32.77	39.62	45.47

2.6.4 Cross Slope and Longitudinal Grade

Both longitudinal grade and cross slope are the key factors to form flow path slope. As Figure 8(a) shows, the maximum longitudinal grade is 12.03%, and the standard deviation is 2.48. Due to the vibration of the surveying vehicle, there is some

noise in the raw cross slope captured by IMU roll angle. Based on the 3D laser imaging data, the vehicle body roll angle can be measured, and then the raw cross slope is calibrated. Figure 8(b) shows the raw cross slope and calibrated cross slopes. Comparing the raw cross slope data and calibrated cross slope, the majority of the noise is eliminated from the raw data through the calibration. The cross slope presents negative values at left turn curves and positive values at right turn curves. In this test site, curves #1, #4, and #5 belong to left turn curve, while curves #2 and #3 belong to right turn curve. The statistical results of the calibrated cross slopes on test site are given as follows: (1) the average cross slope on the straight road segments is 1.94%; (2) the average cross slope of curve #1, #2, #3, #4, and #5 are -2.06%, 4.96%, 5.80%, -3.81%, and -5.01%, respectively.

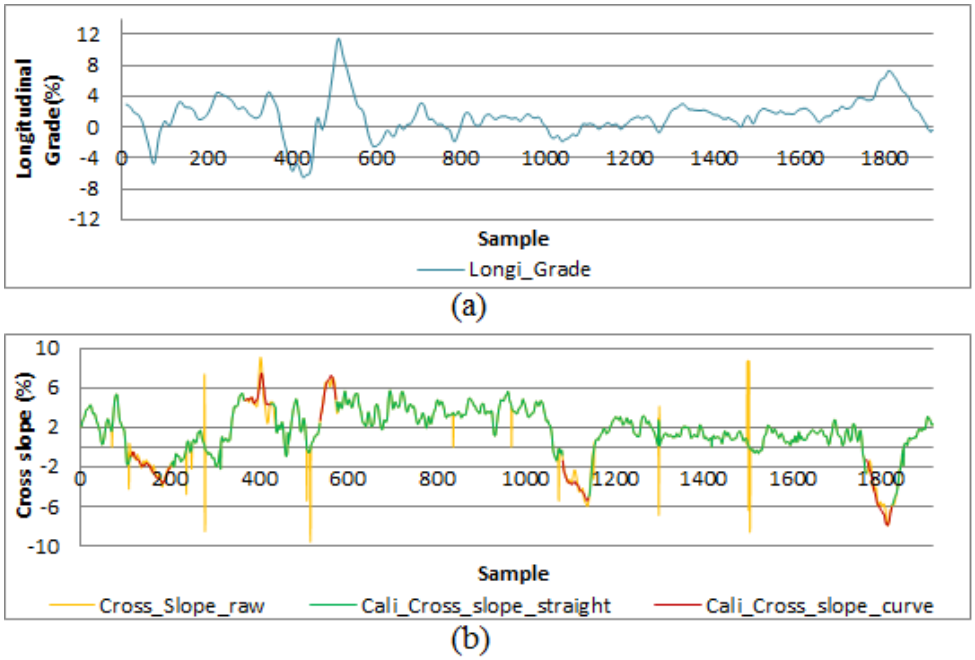

Figure 8 Geometry of Test Site: (a) Longitudinal Grade; (b) Cross Slope

2.6.5 EMTDs and WFDs

Figure 9(b) shows the EMTDs at the test section, with an average value of 1.20 mm, and Figure 9(a) shows the corresponding WFD along the test section, with an average value of 1.73mm and the maximum value of 8.52 mm. The WFD is calculated with Gallaway WFD model based on pavement texture depth, flow path slope, and local rainfall intensity as inputs.

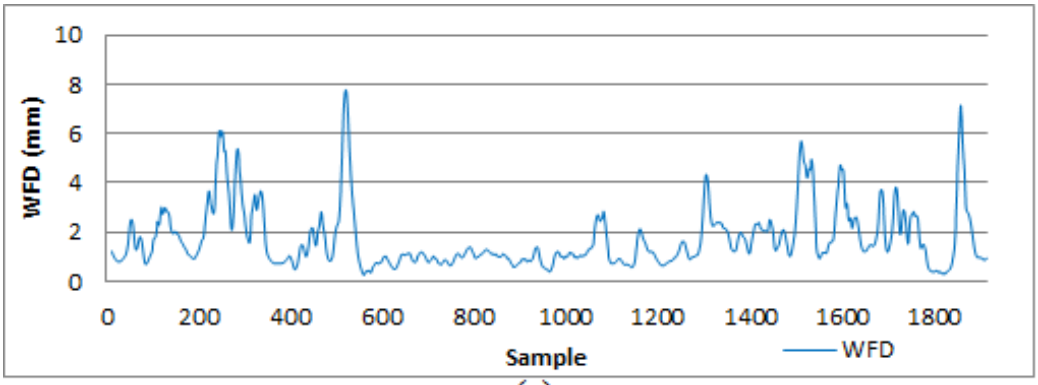

(a)

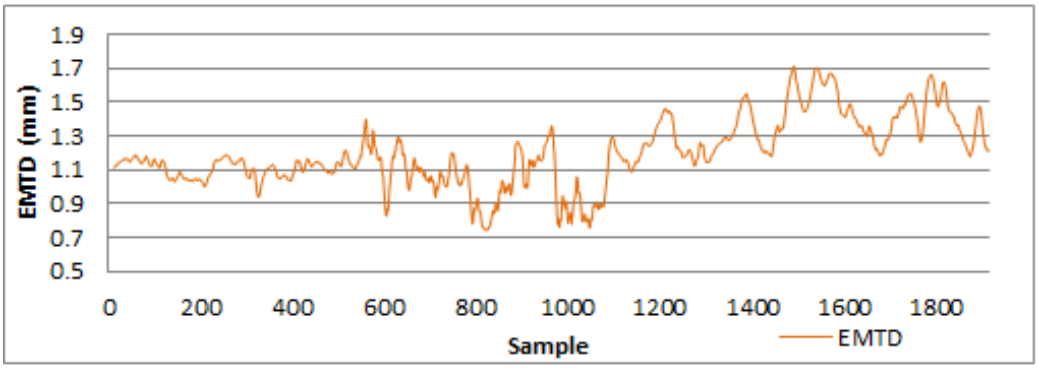

(b)

Figure 9 WFDs and EMTDs of Test Site: (a) WFDs; (b) EMTDS.

2.6.6 Hydroplaning Speed Estimation

13 samples of the calculated WFD, EMTD and IMU data for hydroplaning speed prediction are given in Table 2.2. Gallaway model, USF model, the improved Gallaway model, and the improved USF model are utilized to predict hydroplaning speed, respectively, as shown in Figure 10(a). Results indicate the predicted hydroplaning speeds from original Gallaway and USF model are approximately 140km/h and 165km/h, respectively, which are around 50km/h higher than those predicted from the improved Gallaway model (96km/h) and improved USF model (91km/h). The results also show as expected that the hydroplaning speeds at curves of the five horizontal curves in Figure 10(a) are lower than that on the straight road sections.

Table 2.2 Samples of 3D Imaging Data and IMU Data for Hydroplaning Speed Calculation

Sample ID	WFD (mm)	EMTD (mm)	Cross Slope (%)	Longitudinal Grade (%)
1	1.64	1.12	2.07	3.27
2	1.51	1.11	2.26	3.18
3	1.35	1.11	2.54	3.10
4	1.30	1.10	2.68	3.12
5	1.23	1.11	2.82	3.07
6	1.21	1.09	2.87	2.89
7	1.13	1.12	2.95	2.78
8	1.05	1.17	3.05	2.77
9	1.03	1.14	3.23	2.72
10	1.00	1.10	3.44	2.67
11	0.93	1.12	3.64	2.71
12	0.94	1.11	3.74	2.81
13	0.94	1.10	3.76	2.85
14	0.86	1.17	3.79	2.79
15	0.92	1.10	3.83	2.76

2.6.7 Potential Hydroplaning Segment Detection

Identification of hazardous locations with hydroplaning potential is based on the comparison of estimated hydroplaning speed with posted speed of the road section (15). At the test site, speed limits are 80km/h on straight sections and 56km/h on road curves. The average hydroplaning speeds calculated with the four models are used to detect potential hydroplaning segments, shown in Figure 10(a). Since the predicted hydroplaning speeds at the five curves are higher than posted speed limit, there is a low hydroplaning risk at the five curves for vehicles operating at speed limit. However, for several segments of the test site, the predicted hydroplaning speeds are lower than the posted speed limit. Therefore, these segments can be identified as potential hazardous segments for hydroplaning risk, as marked with red line in Figure 10(b). To minimize traffic accidents caused by hydroplaning, highway agencies can post a reduced speed sign at these locations, or take other remedial actions, such as installing High-Friction Surface Treatment (HFST) (26).

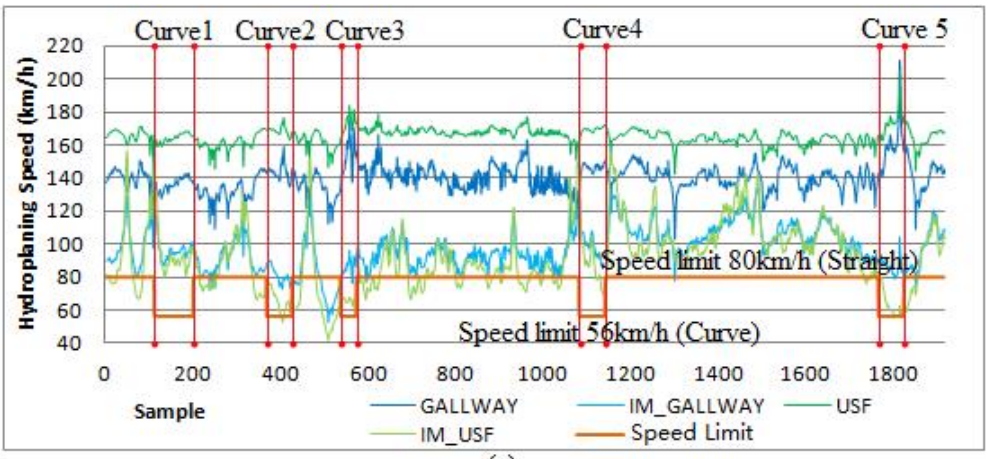

(a)

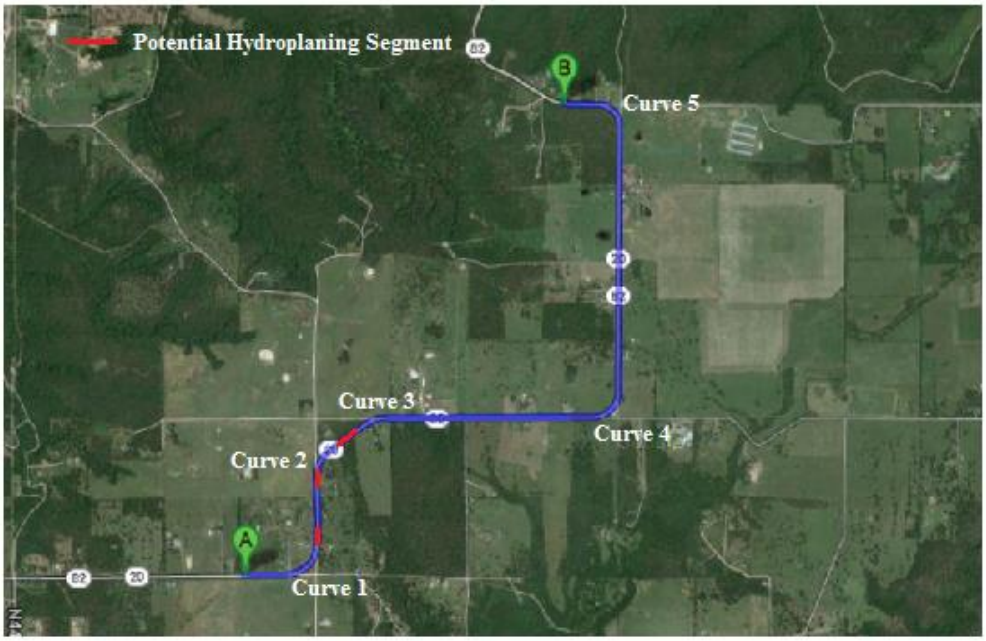

(b)

Figure 10 Hydroplaning Test Site: (a) Hydroplaning Speed; (b) Hazardous Segments

2.7 Conclusions

To take into account the effects of flow path slope on vertical wheel load perpendicular to pavement surface and the resulting hydroplaning speed, the Gallaway and USF models are modified for improvements in this study. The sensitivity analysis shows that the hydroplaning speed is more sensitive to cross slope than longitudinal grade in the improved models. A volumetric measuring method is used to calculate Estimated MTD based on the entire lane data. IMU data and 3D laser imaging data are combined together to realistically model vehicle movements on cross slopes. Local

rainfall intensity is obtained from NOAA precipitation database. By considering effects of cross slope and longitudinal grade on wheel load and flow path length, it is found that hydroplaning speed decrease with the increase of the longitudinal grade, but increase with the increase of the cross slope. The improved models provided lower hydroplaning speed than original Gallaway and USF models. An important future work is to use a combined slope based on longitudinal grade and cross slop to demonstrate the validity and effectiveness of the improved models.

3. WAVELET BASED MACRO-TEXTURE ANALYSIS FOR PAVEMENT FRICTION PREDICTION

3.1 Introduction

3.1.1 Background

Pavement friction is the force resisting the relative motion between the vehicle tire and pavement surface, and it is a critical factor influencing the crash ratios on both wet and dry conditions for roads (27 and 28). Pavement friction data is primarily measured using the British Pendulum Tester or Dynamic Friction Testers for static testing, Grip Tester or Locked-wheel Skid Tester for high-speed testing. All the existing testing devices consume water and testing tires for pavement friction data collection. Therefore it could be expensive for agencies to collect pavement friction data at the network level. Due to the limit of water tank volume used in friction measurement, current skid resistance survey is generally performed at the project level. In addition, the existing friction measurements require physical contact between testing tires/sliders and pavement, which only covers a small portion of a pavement surface. Because of potential traffic wandering, friction data are not measured following the same path and thus data variations are acquired for long term friction monitoring.

Pavement texture is defined as the deviations of pavement surface from a true planar surface, and normally two types of surface texture affect wet pavement friction: microtexture (wavelengths of 1 μm to 0.5 mm) and macro-texture (wavelengths of 0.5 mm to 50 mm) (29). Pavement microtexture is normally collected in laboratory statically through high resolution devices, while pavement macro-texture is measured via sand patch test, Circular Track Meter, or High Speed Profiler in terms of Mean Texture Depth (MTD) and/or Mean Profile Depth (MPD) in the field. Various studies have been conducted to correlate pavement friction with pavement texture indicators. Various parameters, such as traffic level, aggregate characteristics, and pavement texture, were considered to develop pavement friction prediction models (30, 31, 32, 33, 34, and 35). Several research activities correlated pavement texture with friction performance using advanced data analysis methodologies (36 and 37). A comprehensive evaluation of field performance for several high friction surface treatment (HFST) sites was conducted and

no direct relationship was found between MPD and friction performance (38). Despite extensive studies conducted in the past decades, the relationship between pavement macro-texture and surface skid resistance has not been fully understood.

3.1.2 Objectives

The objectives of this section are to implement discrete wavelet transform to decompose pavement surface macro-texture profile into multi-scale characteristics and investigate their suitability for pavement friction prediction. The pavement macro-texture profiles collected on six HFST sites in Oklahoma are decomposed. Two types of energy indicators, Total Energy (TE) and Relative Energy (RE), are calculated from the decomposed macro-texture profiles to represent the characteristics of macro-texture at various wavelengths. Subsequently multivariate linear regression analysis is conducted to examine the potential relationships between pavement friction and the energy indicators derived from the pavement macro-texture data.

3.2 Methodology

Wavelet is an irregular and asymmetric waveform within limited duration that has an average value of zero, and it can be stretched or compressed to match signal at different locations and scales and therefore represent signal in frequency and time domain simultaneously (39). Wavelet transform has been widely used in many civil engineering applications, such as damage detection (40), corrosion detection (41), crack detection (42), effectiveness evaluation of pavement maintenance treatments (43, 44, and 45), and pavement macro-texture profile analysis (46 and 47).

Discrete wavelet transform is applied herein to decompose pavement macro-texture profiles into multi-level decompositions in the form of approximation signal and detailed signals. The macro-texture profile can be represented as a series of profiles corresponding to distinct wavelength sub-bands (47):

$$s(t) = a_L(t) + Sum_j[d_j(t)] \quad (3.1)$$

Where Sum_j is the summation in terms of j, $a_L(t)$ is the approximate signal corresponding to the longer wavelength, $d_j(t)$ is the detail components relating to the shorter wavelength at level j, and L is the number of sub-bands or decomposition levels.

After profile decomposition, the energy of each decomposition level can be employed to interpret pavement macro-texture profile at various scales (43 and 47). The energy content for a particular decomposed sub-band is obtained as below (47):

$$E_j^d = Sum_i\{|d_j(x)|^2\} \quad (3.2)$$

Where Sum_j is the summation in terms of j, E_j^d and $d_j(x)$ are the wavelet energy indicator and detail coefficients for the jth decomposition level of a macro-texture profile, and N is the number of data points in the decomposed macro-texture profile. Specifically, the total energy (TE) of given macro-texture profile is the summation of E_j^d from the first to the L^{th} sub-band and can be calculated as (47):

$$TE = Sum_j\{E_j^d\} \quad (3.3)$$

The relative energy (RE) is the percentage of the energy at the j^{th} decomposed sub-band as compared to the total energy (47):

$$RE_j = (E_j^d)/TE \times 100\% \quad (3.4)$$

The RE_j at various sub-bands constitute the energy distribution of a given macro-texture profile at different wavelengths.

3.3 Data Collection and Preliminary Results

3.3.1 Data Collection

HFST has gained its popularity in recent years in the United States with proved capability in improving pavement friction, decreasing crash frequency and thus roadway safety particularly at horizontal curves (48 and 49). The data collection in this section includes macro-texture and friction testing of two HFST sites on Interstate 40 (I-40), one HFST site on Interstate 44 (I-44) and three HFST sites on State Highway 20 (SH-20) in Oklahoma. The existing pavements on I-40, I-44, and SH-20 were constructed with stone matrix asphalt (SMA), Portland cement concrete (PCC), and conventional hot mix asphalt (HMA) respectively. HFST were installed on all the three traffic lanes in the east bound of I-40 and the west bound of I-44, while one lane for both directions on SH-20. Considering different traffic directions and number of lanes of these HFST sites, 15 data collections were conducted in November 2015 and the detailed information for each site is summarized in Table 3.1.

Table 3.1 HFST Sites for Data Collection

Data Collection ID	Site ID	Site Location	Lane /Direction	Abutting Pavement	AADT	Functional Class	Radius (M)	Grade (%)
1	Site 1	I-40EB	Right	SMA	64,678	Interstate	2,000	-2.5
2	Site 1	I-40EB	Middle	SMA	64,678	Interstate	2,000	-2.5
3	Site 1	I-40EB	Left	SMA	64,678	Interstate	2,000	-2.5
4	Site 2	I-40EB	Right	SMA	64,678	Interstate	2000	-1.5
5	Site 2	I-40EB	Middle	SMA	64,678	Interstate	2000	-1.5
6	Site 2	I-40EB	Left	SMA	64,678	Interstate	2000	-1.5
7	Site 3	I-44WB	Right	Concrete	129,000	Interstate	2000	-2.0
8	Site 3	I-44WB	Middle	Concrete	129,000	Interstate	2000	-2.0
9	Site 3	I-44WB	Left	Concrete	129,000	Interstate	2000	-2.0
10	Site 4	SH-20	North	HMA	390	Minor Arterial	400	3.5
11	Site 4	SH-20	South	HMA	390	Minor Arterial	400	3.5
12	Site 5	SH-20	North	HMA	390	Minor Arterial	500	3.0
13	Site 5	SH-20	South	HMA	390	Minor Arterial	500	3.0
14	Site 6	SH-20	North	HMA	390	Minor Arterial	200	-3.5
15	Site 6	SH-20	South	HMA	390	Minor Arterial	200	-3.5

Pavement macro-texture profiles were collected using the AMES 8300 Survey Pro High Speed Profiler along the left wheel-path at traffic speed. MPDs were calculated based on ASTM standard (50) for each macro-texture profile measurement. Grip Tester, which has been used in recent years by Federal Highway Administration (FHWA) on many demonstration projects in the United State, was utilized to collect friction data along the same wheel-path. The friction numbers were reported for each data collection to represent the pavement surface skid resistance conditions. To determine the effectiveness of HFST in improving surface properties, all the data sets are collected beginning 100 m to 150 m before and through 100 m to 150 m after each HFST section.

3.3.2 Preliminary Results

Friction numbers and MPD values were obtained at 1 meter (3 feet) interval for the HFST sites. Examples of pavement friction number and MPD data are shown in Figures 11 and 12 to demonstrate pavement friction and macro-texture conditions for these sites.

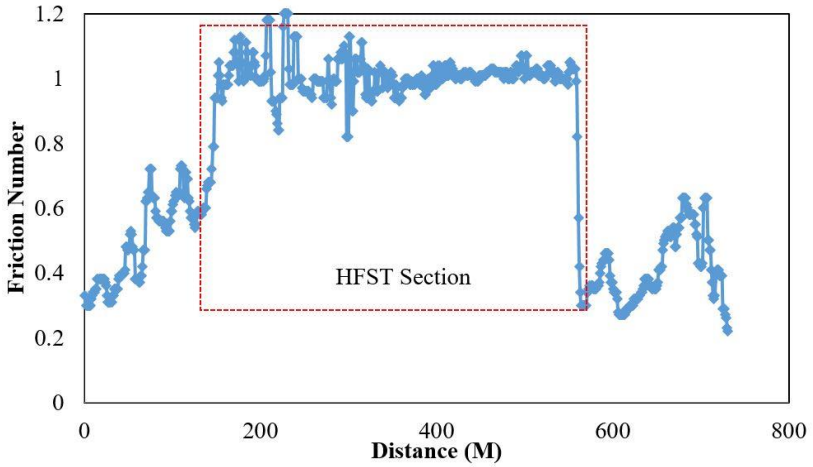

(a) Friction

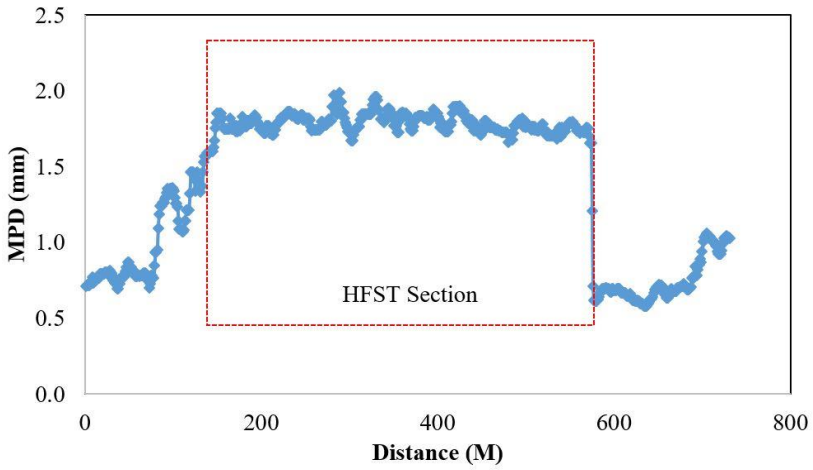

(b) MPD

Figure 11 Example Site with Distinct Friction and MPD (Data Collection #7)

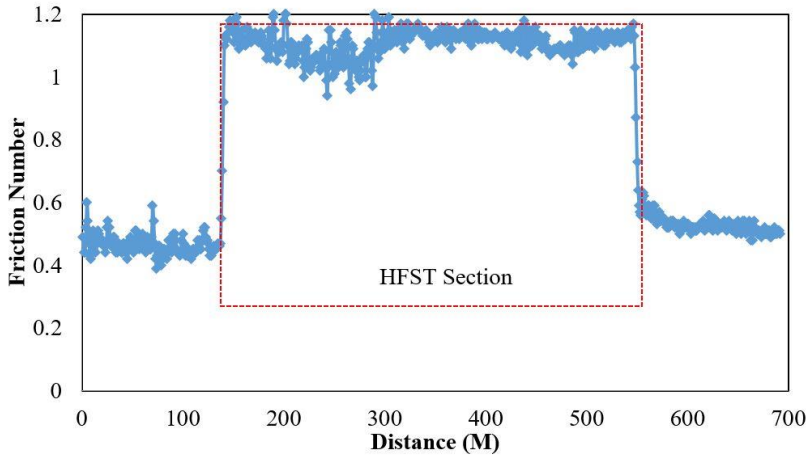

(a) Friction

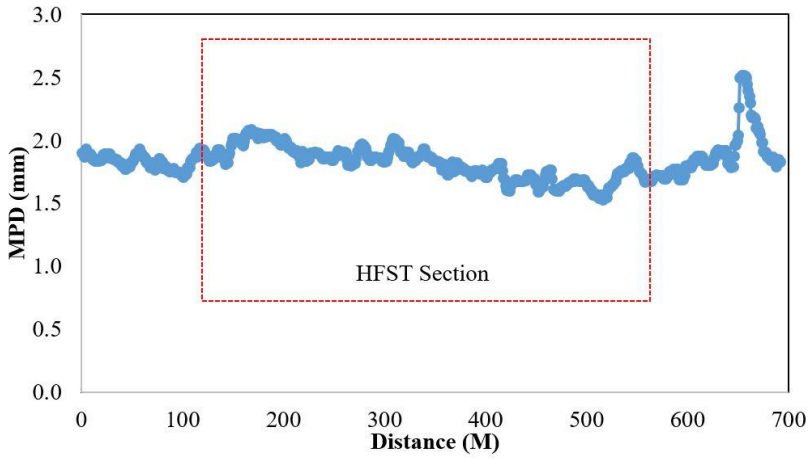

(b) MPD

Figure 12 – Example Site with Distinct Friction Only (Data Collection #1)

All sites show clear improvement of skid resistance and differentiation of the HFST section from the abutting pavements for all the data collections (Figures 11(a) and 3.2(a)). The average friction number on HFST sections is 1.00, while the friction number of abutting pavement surfaces without HFST has an average of 0.50. The differences of MPD between the HFST sections and adjacent pavements vary among these data sets. For example, MPD values of Collection #7 are much higher on HFST section in contrast to those on the abutting concrete pavement (Figure 11(b)), whereas MPDs of Collection #1 don't show noticeable difference between the HFST section and its adjacent pavement (Figure 12(b)). On average, the mean value of MPD on the HFST

sections is 1.70 mm, while the MPDs of the regular pavement surfaces has an average of 1.34 mm.

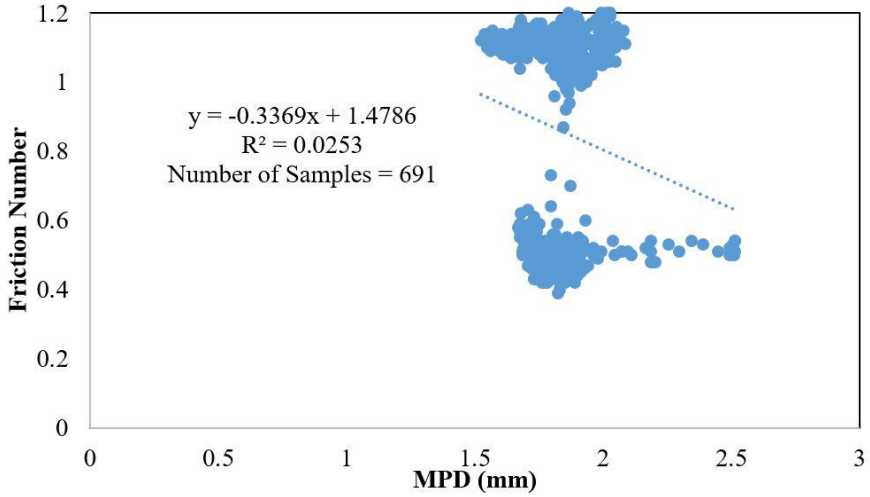

Figure 13 Scatter Plot of Friction Number and MPD (Data Collection #1)

The scatter plot between friction numbers and the corresponding MPDs of Collection #1 are demonstrated in Figure 13. For the 691 pairs of friction number and MPD values, the R-squared value of the regression is approximately to zero, which indicates that no direct relationship can be developed solely between pavement friction number and MPDs.

3.4 Wavelet Analysis of Macro-texture Profiles

In this study, a Daubechies wavelet of order 3 (db3) is selected as the mother wavelet to decompose the collected macro-texture profiles. Daubechies wavelets are compactly supported orthonormal wavelets that make discrete wavelet analysis practicable. The Daubechies wavelets are denoted as dbN, where N is the order, and db the “surname” of the wavelet. The Daubechies family has ten members from db1 to db10. In particular, the db3 wavelet is widely employed by researchers as the mother wavelet to analyze pavement surface data since it contains more localized spikes to better represent typical pavement roughness/texture profiles (43, 46, 47, and 51). Subsequently, TE and RE are calculated every 1.0 meter and compared among the four pavement types to reveal the distinct characteristics of macro-texture composition.

With the sample interval of 0.483 mm (0.02 inches) for the obtained macro-texture profiles, there are 2072 data points for every 1 meter of macro-texture profile,

which requires a total of 11 decomposition levels for wavelet analysis (211 = 2048). However it is widely accepted that the upper bound of macro-texture wavelength is 50 mm (29), and therefore only seven decomposition levels, denoted as Level 1 (D1) through Level 7 (D7), are considered in this section to calculate TE and RE at 1.0 meter interval for the macro-texture profiles.

3.4.1 Total Energy Analysis

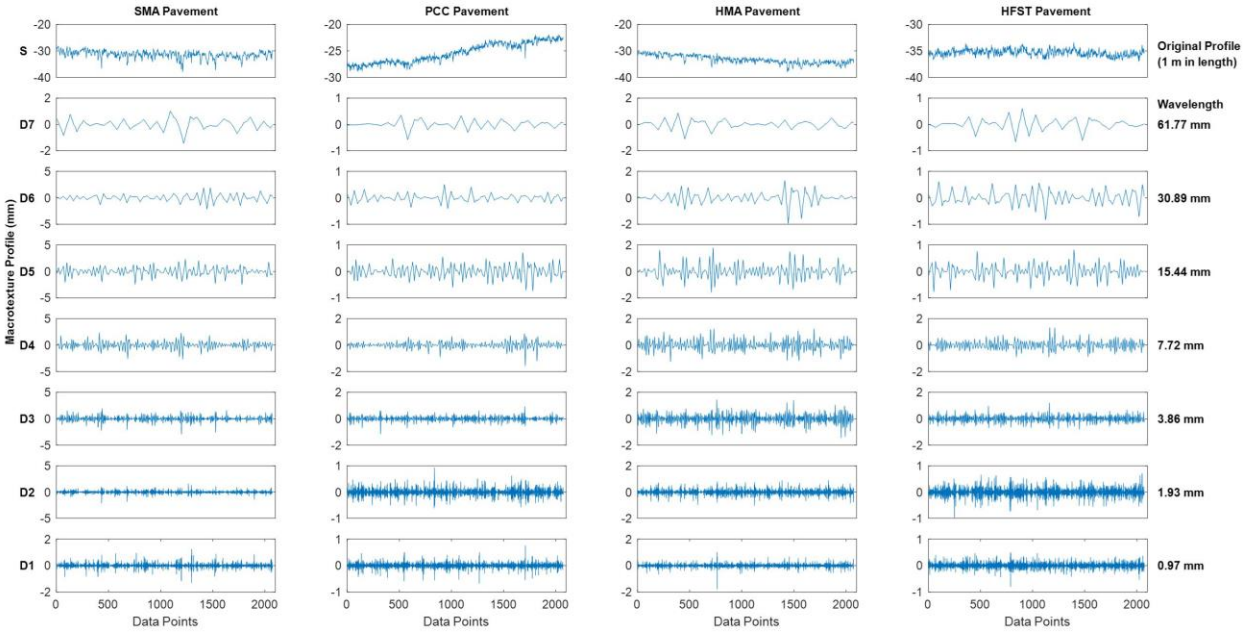

Figure 14 Wavelet Decompositions of Macro-texture Profiles

The original macro-texture profiles and the decomposed macro-texture profiles for the seven decomposition levels are shown in Figure 14. In total there are four types of pavement surfaces in the data collection, including the three existing surfaces (hot mix asphalt – HMA on SH20, stone-matrix asphalt – SMA on I40, Portland cement concrete – PCC on I44) and the HFST on these sites. For the j^{th} decomposition results, the horizontal axis shows the number of data points and the vertical axis represents the amplitude of pavement macro-texture profiles. The equivalent wavelengths for each decomposition level are provided on the right margin of the figure.

The energy distribution for each decomposition level of the macro-texture profiles for the four pavement surface types are calculated and provided in Figure 15. The overall TE on SMA, HMA, HFST, and PCC pavement are 2,254, 1,532, 1,401, and 337 mm2 respectively. The sequence of the overall TE among the pavement categories

agrees well with the coarseness level of pavement macro-texture profiles observed from Figure 14. The number in the bracket of the x-axis is the corresponding wavelet length of each decomposition level. For friction, the average friction numbers are 0.50, 0.56, 1.0, and 0.40 for the SMA, HMA, HFST, and PCC pavements. Therefore, a pavement section with coarser macro-texture doesn't guarantee a higher pavement friction number. For example, the total energy of the HFST sections is 1401 mm^2, which is not the maximum among the four pavement surfaces, while it has the highest friction number.

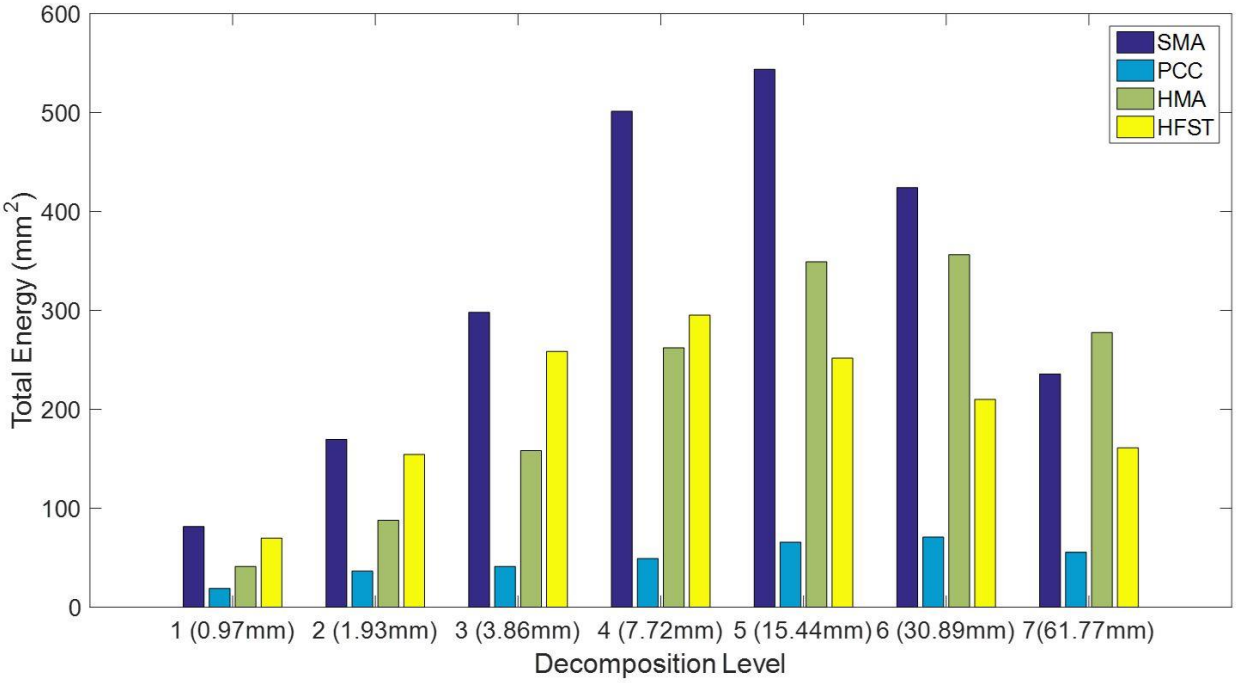

Figure 15 Energy Distribution

3.4.2 Relative Energy Analysis

Considering the wide range of wavelength (0.5~50 mm) for macro-texture, pavement macro-textures at various wavelengths may have different contributions to pavement friction performance. Therefore, it's necessary to investigate the relative energy distribution of macro-texture profiles at each decomposition level and how it impacts the friction performance for different pavement surface types. The cumulative RE distribution at each decomposition level is shown in Figure 16.

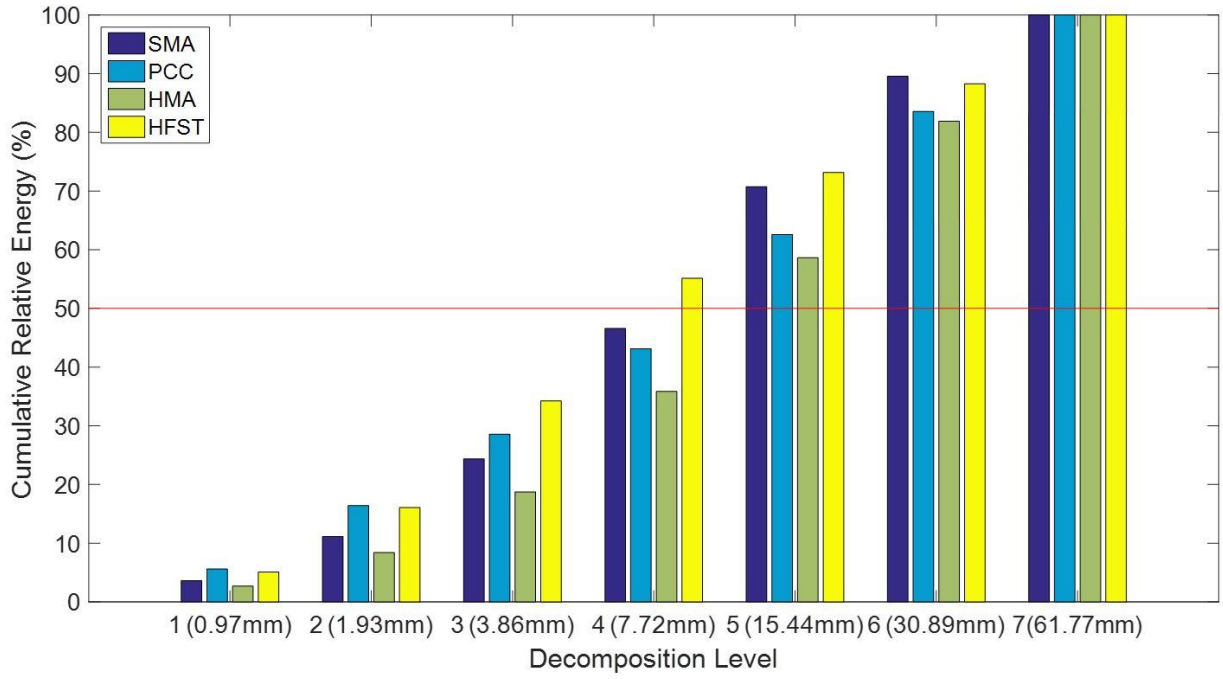

Figure 16 Cumulative Relative Energy Distribution

It is noticed that (1) more than 50% of energy of macro-texture on HFST sections stores within the first four decomposition levels, which correspond to wavelengths ranging from 0.97 mm to 7.72 mm; (2) while more than half of the energy of the macro-textures for the other three pavement types distributes within the last three decomposition levels, which correspond to wavelengths from 15.44 mm to 61.77 mm.

Table 3.2 Correlation Coefficients between RE and Friction Number

Site ID	D1	D2	D3	D4	D5	D6	D7
1	0.93	0.95	0.94	-0.21	-0.86	-0.74	-0.02
2	0.06	0.35	0.76	0.58	-0.34	-0.33	-0.37
3	-0.39	0.12	0.79	0.86	0.26	-0.57	-0.45
4	0.29	0.52	0.83	0.79	-0.39	-0.77	-0.55
5	0.58	0.68	0.76	0.50	-0.65	-0.63	-0.47
6	0.81	0.84	0.73	-0.19	-0.75	-0.62	-0.05

Subsequently, correlation analysis between relative energy of macro-texture at various decomposition levels and friction number is performed. The correlation coefficients are summarized in Table 3.2 for each site. Correlation coefficient with zero means that there is no correlation, -1 denotes a perfect negative correlation, while +1 suggests a perfect positive correlation between the two variables. For these six sites, the correlation coefficients between REs and friction number are negative from the 5th

to the 7th composition levels (D5 to D7) (except D5 at Site 3), and positive from the 1st to the 3rd composition levels (D1 to D3) (except D1 at Site 3). In other words, the pavement friction performance improves with macro-texture at wavelength from 0.97 mm to 3.86 mm while decreases with macro-texture at wavelength from 15.44 mm to 61.77 mm. The correlation coefficient between the relative energy at the 4th composition level (D4) and friction number varies among the sites, which indicates that the contribution of pavement macro-texture at the wavelengths between 3.86 mm and 7.72 mm to pavement friction is inconsistent and depending on the pavement surface type.

3.5 Friction Prediction Model

The collected macro-texture profiles and friction data of Collection #1, #7, and #12 are selected to represent various pavement types (SMA, HMA, PCC and HFST) as the data set for friction prediction model development. Multivariate linear regression is performed to predict friction number based on the TE and RE of the selected pavement macro-texture profile:

$$\text{Friction Number} = a + TE \times b + \text{Sum}_j(RE_j \times c_j) \quad (3.5)$$

Where a, b, and c_j are the estimated coefficients for intercept, TE and RE_j separately. The estimated regression coefficients and corresponding P-values of the multivariate model are summarized in Table 3.3. All P-values of TE and RE_j herein are smaller than 0.05, indicating their significances to pavement friction.

Table 3.3 Estimated Coefficients and P-value for Friction Prediction Model

Item	Intercept	TE	RE_1	RE_2	RE_3	RE_4	RE_5	RE_6	RE_7
Coefficient	0.142	6.34E-05	0.092	-0.113	0.1	0.004	-0.039	0.01	0.016
P-value	0.042	6.03E-06	0.007	0.006	0.003	0.003	0.002	0.001	0.001

Based on the developed coefficients, all the macro-texture profiles of the 15 data collections are used to predict the friction numbers and validate the proposed model by comparing the measured and predicted friction numbers. The statistic result of the comparison for each data collection is summarized in Table 3.4. The number of friction data samples ranges from 358 to 1184 for each data collection. R-squared values range from 0.42 to 0.93, with the highest R squares for I-40 sections, followed by I-44 and SH-20.

Table 3.4 Statistic Result of Comparison between Measured and Predicted Friction Number

Highway	Site ID	Collection ID	R^2	SSE	No. of Points
I-40	Site 1	1	0.93	2	654
I-40	Site 1	2	0.90	4	628
I-40	Site 1	3	0.83	4	750
I-40	Site 2	4	0.85	3	584
I-40	Site 2	5	0.84	4	597
I-40	Site 2	6	0.79	6	607
I-44	Site 3	7	0.79	7	621
I-44	Site 1	8	0.62	13	618
I-44	Site 3	9	0.78	11	610
SH-20	Site 4	10	0.71	10	358
SH-20	Site 4	11	0.79	5	402
SH-20	Site 5	12	0.53	5	361
SH-20	Site 5	13	0.78	3	510
SH-20	Site 6	14	0.67	9	1184
SH-20	Site 6	15	0.42	8	700

The examples of measured and predicted friction numbers with the highest (Collection #1 of Site #1 on I-40) and the lowest (Collection #15 of Site #6 on SH-20) R-squared values are shown in Figure 17. Site 1 locates on I-40 with moderate horizontal curve, minimum longitudinal grade, and minor distress on the existing surface, while Site 6 locates on SH-20 with sharp horizontal reverse curves, steep longitudinal grades, and significant amount of defects on the existing pavement. For data collections on sharp curves with the existence of lateral gravity forces, centrifugal forces, and possible consistent acceleration/deceleration of the data collection vehicle, the friction and macro-texture data collected generally show significant higher variabilities, resulting in the low R-squared values in the models.

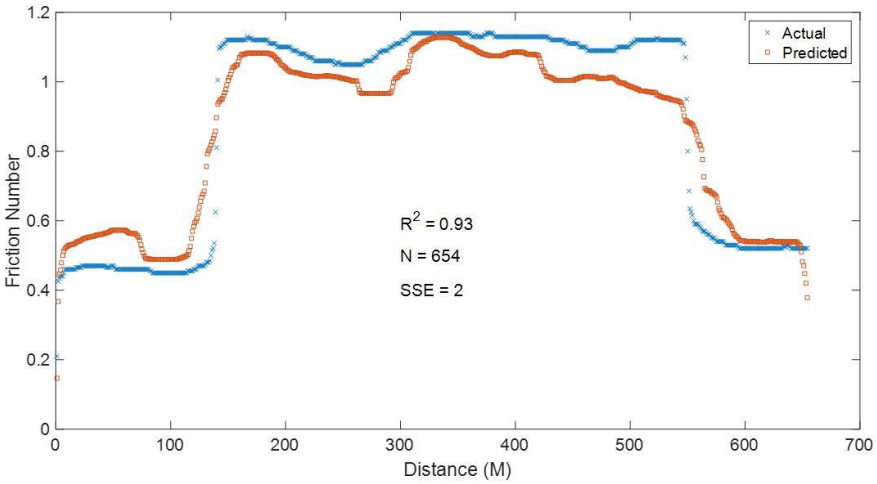

(a) Prediction with the Highest R-squared Value (Collection #1)

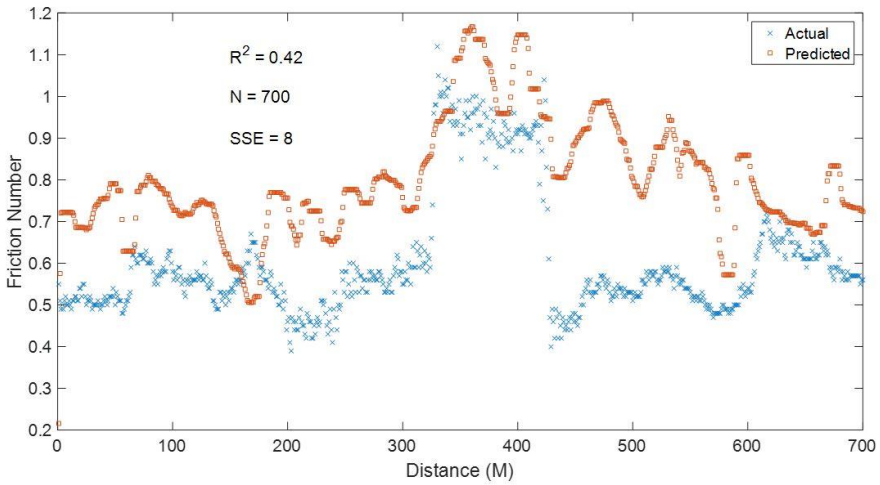

(b) Prediction with the Lowest R-squared Value (Collection #15)

Figure 17 Pavement Friction Prediction Results

It should be emphasized that the quality of texture and friction data is critical for a robust model development. HFST Site #1 was installed on moderate curves on asphalt pavement surface, and the adjacent pavement had minor pavement surface distress. The data collected on Site #1 exhibits high repeatability and consistency among the data collection on the multiple lanes. Therefore, the regression friction models have high R-squared values on Site #1. HFST Sites #2 and #3 were installed on bridge decks with existing asphalt and concrete surfaces on slightly curved highways. Even though minor distress were observed before installation, faulting along the slab joints on the deck are noticeable. As a result, the macro-texture and friction data contain significant amount of

data points with abnormal measurement values especially along the joints. Significant vehicle vibrations were observed when vehicle moving on the transition section between pavement and bridge deck. Due to the vehicle excitation, the repeatability and consistency of friction and macro-texture data collection on Site #2 and Site #3 are not as consistent as those collected on Site #1. Accordingly, the regression models have lower R-squared values as compared to those for Site #1.

Sites #4 to #6 are located on SH-20 on a low volume roadway but with compound sharp horizontal curves and longitudinal grades. In addition, the existing pavements had experienced extensive crack sealing and rutting on the surface. The data sets collected on these sites have the lowest repeatability and consistency, leading to the low levels of R-squared values.

3.6 Conclusions

In this section, pavement macro-texture and friction data from six HFST sites that were installed on existing SMA, PCC, and HMA pavement surfaces are analyzed. 15 pairs of pavement macro-texture and friction data were collected with length ranging from 358 m to 1184 m considering the number of lanes and traffic directions of the sites. Total energy and the relative energy distributions are calculated for the decomposed macro-texture profiles from wavelet transform, and the relationship between the energy indicators and pavement friction performance is studied. Pavement friction prediction model is developed based on multivariate linear regression method incorporating energy indicators of pavement macro-texture.

The average MPD and friction numbers on HFST sections are 1.70 mm and 1.00 respectively, while the MPD and friction numbers of non-HFST surfaces have the average of 1.34 mm and 0.50. For Site #1 and #2, the friction data is significantly higher on HFST sections than those on adjacent SMA pavements, whereas the MPD values exhibit minor difference between HFST and existing pavement surface. Even though it is widely accepted that pavement skid resistance is tied to surface macro-texture, MPD alone is not adequate for pavement friction prediction.

The energy distributions for macro-texture on the different pavement surfaces could vary significantly. On HFST sections, more than 50% of the energy is distributed within the 1st to the 4th decompositions levels (D1 to D4), with the wavelengths ranging

from 0.97 mm to 7.72 mm. While for the other three pavement surface types, including SMA, PCC, and tradition HMA, more than 50% of the energy of macro-texture profiles is distributed within the 5th to the 7th decomposition levels (D5 to D7) with longer wavelengths ranging from 15.44 mm to 61.77 mm.

Seven decomposition levels are considered in this section for macro-texture analysis. All the energy indicators for the seven levels show significant contributions to the pavement friction performance, which are used as the independent variables for friction model development. The energies at wavelengths from 0.97 mm to 3.86 mm contributes positively to pavement friction while those at wavelengths from 15.44 mm to 61.77 mm demonstrates negative impacts.

Pavement surface conditions and the geometric characteristics of the roadway could significantly impact the repeatability and the accuracy of macro-texture and friction data measurements. For example, Sites #4 to #6 located on a low volume road with sharp horizontal curves, steep longitudinal grades and extensive cracking and defects on the existing surfaces, the macro-texture and friction data collected on these sites show extensive variations with many abnormal data points, therefore the proposed friction prediction model on these sites are less robust comparing to the results from other sections.

4. NOVEL MACRO- AND MICRO-TEXTURE INDICATORS FOR PAVEMENT FRICTION USING HIGH-RESOLUTION 3D SURFACE DATA

4.1 Introduction

4.1.1 Background

Pavement friction is the force resisting the relative motion between the vehicle tire and pavement surface, and pavement texture is defined as the deviations of the pavement surface from a true planar surface (27). Pavement friction can be measured using British Pendulum Tester, Dynamic Friction Tester, Locked-Wheel Skid Trailer, or the Wehner/Schulze equipment statically or dynamically (19, 52, 53, and 54). Pavement macro-texture can be evaluated in terms of mean texture depth (MTD) or mean profile depth (MPD) via sand patch, circular track meter, or high speed profiler (16, 17, and 55). Micro-texture of aggregates or pavement coring samples can be characterized using high resolution devices in the laboratory and evaluated by various methods such as imaging analysis (30, 34, 56, and 57). It is widely agreed that pavement macro- and micro-texture are the primary contributors to pavement friction performance at high and low traffic speeds (29). However, thus far no consistent relationships have been developed for pavement texture and friction if depending on the widely used traditional texture indicators, such as MPD and MTD (38).

With the development of non-contact 3-Dimensioal (3D) measurement technologies and the improvement in the computing and processing power of computers in the past decades, it is feasible and desirable to describe road surface texture in both macro- and micro-scale under 3D at high resolution. These 3D based indices and parameters not only promise a quantum leap in describing road surface texture characteristics, but also provide in-depth understanding of the relationship between texture and friction for the purpose of replacing existing costly friction measurement methodologies. Using new texture parameters which are highly relevant to wet pavement friction could aid in the screening of road network and identifying road segments requiring investigative friction measurements.

Various processing technologies have been applied to analyze 2-Dimensional (2D) or 3D pavement texture profiles for the development of new texture indicators.

Wavelet analysis, Hilbert-Huang transform, fractal analysis, and the power spectra density methodology were some of the examples used to characterize pavement macro-texture and relate pavement surface macro-texture attribute to friction performance (37, 47, 58 and 59). Other studies measured 3D pavement macro-texture data in the field via high-speed laser scanners using a wide range of texture indicators and evaluated their relationships with pavement friction performance (60 and 61). There has been limited research to investigate the relationship between pavement friction and micro-texture based on 2D pavement profiles or 3D images with resolution up to 0.015 mm; however, they relied on traditional texture parameters and failed to identify the proper texture parameters to predict pavement friction performance (62, 63, 64 and 65). Therefore, understanding the relationship between macro- and/or micro-texture and friction performance under 3D conditions using proper 3D texture parameters deserves further research.

In this paper, a wide variety of 3D areal surface parameters are investigated, which are typically grouped into field parameters and feature parameters. The first group of parameters is calculated by taking every data point measured on a 3D areal surface into account, while the second group only considers specific points, lines or areas which are identified as features such as peaks and valleys (66). Field parameters can be further categorized into height parameters, function related parameters, hybrid parameters, and spatial parameters; while feature parameters generally contain peak density, peak curvature, motif slope, significant heights, and morphological parameters (66). According to the definition in ASTM E1845-15 (67), the currently widely used macro-texture parameters, MPD and MTD, belong to the height parameter family and only reflect one attribute of the pavement surface texture. It is necessary to perform a comprehensive evaluation of pavement texture via various available 3D areal parameters, and investigate their contributions to pavement friction performance at both macro- and micro-levels.

4.1.2 Objective

The objective of this section is to identify proper 3D areal texture parameters with good representation to friction performance, and develop corresponding pavement friction prediction models based on the selected 3D areal texture parameters. The Long

Term Pavement Performance (LTPP) Specific Pavement Study 10 (SPS-10) testing site in Oklahoma, including six warm-mix-asphalt (WMA) sections, is selected as the field testing bed. Pavement friction and texture data were collected via a Dynamic Friction Tester (DFT) and a portable 3D laser scanner with ultra-high resolution up to 0.05 mm and 0.01 mm in the lateral and the vertical directions, respectively. Twenty-four 3D areal parameters covering all categories of available texture indicators are calculated for each 3D measurement.

Correlation analyses of those 3D parameters are conducted to exclude those who exhibit strong correlations and remove the potential multicollinearity for regressional friction model development. Subsequently multivariate analysis is performed to develop the relationship between the selected 3D texture parameters and DFT friction data at different testing speeds.

4.2 Field Data Collection

4.2.1 LTPP SPS-10 Testing Site

Table 4.1 Experiment Design for LTPP SPS-10 Site in Oklahoma

Section ID	Binder	Mix	Aggregate Combination	Insoluble Residue (%)
1	PG 70-28	HMA with RAP + RAS	1	56.3
2	PG 70-28	WMA Foaming with RAP + RAS	1	56.3
3	PG 70-28	WMA Chemical with RAP + RAS	1	56.3
4	PG 64-22	WMA Chemical with RAP + RAS	1	56.3
5	PG 58-28	WMA Chemical with RAP + RAS	1	56.3
6	PG70-28	WMA Stone mix with mineral filler	2	43.6
Mainline	PG70-28	HMA with RAP	3	60.8

Note: (1) Aggregate Combination 1 contains 38% 5/8 Chips + 35% Stone Sand + 12% Sand + 12% RAP + 3% RAS; (2) Aggregate Combination 2 contains 90% 5/8 Chips + 10 Mineral Filler; (3) Aggregate Combination 3 contains 34% 5/8 Chips + 13% Scrns. + 30% Stone Sand + 13% Sand + 10% RAP.

The Long Term Pavement Performance (LTPP) recently initiated the Specific Pavement Study 10 (SPS-10) to evaluate the short and long term performance of WMA mixtures in relative to the conventional hot mix asphalt (HMA). The experimental matrix includes, at a minimum, one HMA control section and two WMA test sections using foaming process and chemical additive with 10-25% RAP and RAS content (68). Under

the SPS-10 experiment initiative, the Oklahoma Department of Transportation (ODOT) constructed six LTPP SPS-10 sections on State Highway 66 (SH-66) in Yukon in November 2015. The annual average daily traffic (AADT) on this road section is 5,900. The average temperature ranges from 35.9 ºF in January to 81.2 ºF in July. This newly constructed site is selected as the testing bed in this study to collect pavement 3D texture and friction data.

(a) Site Location (Google Map)

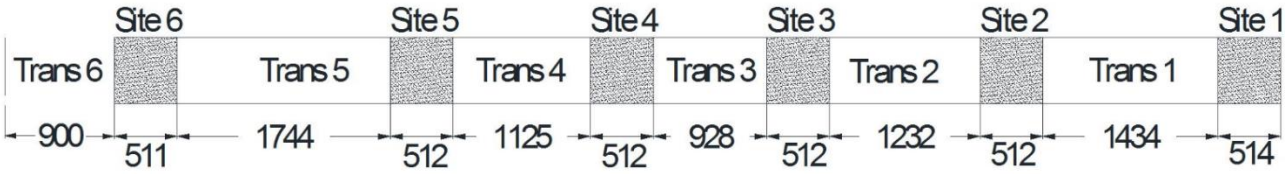

(b) Site Layout (Unit: ft)

Figure 18 LTPP SPS-10 Site in Oklahoma

Table 4.1 lists the experiment design for the SPS-10 sections, and Figure 18 shows the site location and the corresponding length for each section. As shown in Table 1, Sections 1 to 3 are the HMA control section, WMA using foaming process and chemical additive, respectively. Sections 4 and 5 are WMA sections constructed using the same aggregate combination as Sections 1 through 3 but with different binder grades. Section 6 is constructed with stone matrix asphalt (SMA) but the same binder as the first three sections. In addition, the aggregates used in Section 6 have distinct different insoluble residue values from those used in the other five sections, as exhibited in Table 4.1.

4.2.2 Data Collection Devices

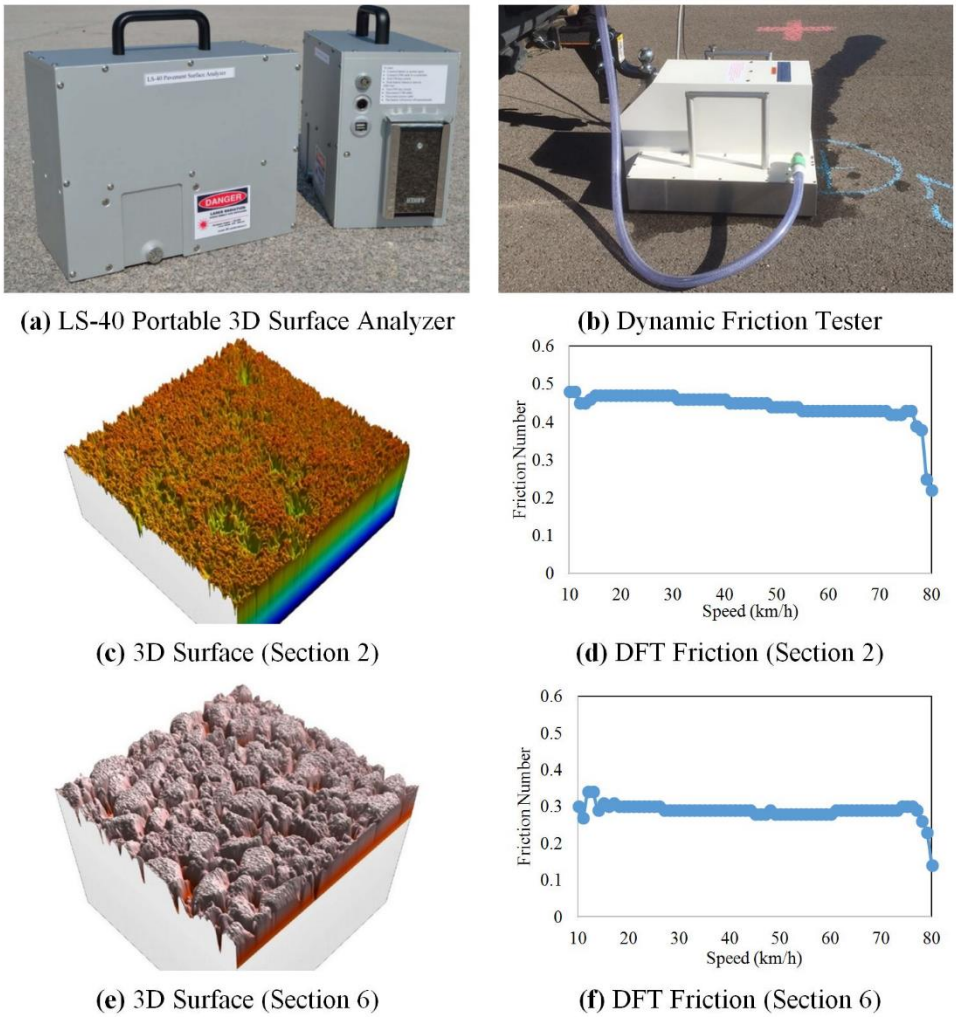

(a) LS-40 Portable 3D Surface Analyzer

(b) Dynamic Friction Tester

(c) 3D Surface (Section 2)

(d) DFT Friction (Section 2)

(e) 3D Surface (Section 6)

(f) DFT Friction (Section 6)

Figure 19 Data Collection Devices and Example Data Sets

A 3D surface measurement and analysis device, named LS-40 Portable 3D Surface Analyzer (Figure 19(a)) (LS-40 for short), scans a 4.5” by 4” pavement surface and collects 3D texture data with height resolution (z) at 0.01 mm and lateral resolution (x, y) at 0.05 mm. LS-40 provides 3D surface data to calculate MPD by processing thousands of profiles over the entire scanned surface according to ASTM-1845 (67) specifications, with optional processing modules of measuring other surface features, such as aggregate form factor, angularity calculation based on multiple contour measurements, and micro-texture indicators, such as Root Mean Square (RMS). LS-40 can not only be used in the laboratory, but also be placed on a localized pavement surface area in the field to collect 2048 by 2448 cloud points for pavement texture

characterization. Figures 19(c) and 19(e) are two example 3D pavement data collected on Section 2 and 6 respectively.

ASTM E1911-09a (52) provides specification on measuring paved surface frictional properties using the Dynamic Friction Tester (DFT). A DFT (Figure 19(b)) consists of a horizontal spinning disk fitted with three spring loaded rubber sliders. The water is sprayed in front of the sliders and a constant load is applied to the slider as the disk rotating on the test surface. The torque is monitored continuously as the disk rotational velocity reduces due to the friction between the sliders and the test surface, then it is used to calculate the surface friction coefficients. DFT has been widely used in friction measurement under various conditions to explore the speed dependency of pavement friction by measuring friction at various speeds. Figures 19(d) and 19(f) are two example DFT friction data measured at the same locations where texture data are collected as demonstrated in Figures 19(c) and 19(e).

4.3 Preliminary Results

The data collection efforts described herein include two data collection activities, the first on November 13th, 2015 immediately after the construction of the testing site and the second on May 25th 2016 when the Sections were approximately 6-month in age, on the six LTPP SPS-10 Sections and the transition sections in-between. LS-40 Portable 3D Surface Analyzer and DFT were used to measure pavement 3D surface data and friction data separately in the right wheelpath (approximately 3.0 ft from the shoulder) in parallel at the same predefined locations. Within each LTPP SPS-10 section, three pairs of LS-40 3D data and DFT friction data were obtained at 100 ft interval starting from the beginning of the section. As the mainline after each LTPP SPS-10 section, another three pairs of pavement texture and friction measurement were conducted at 300 ft interval from the ending of the section. Therefore, thirty-six pairs of pavement 3D texture and friction data measurement were obtained for each data collection. Finally, sixty-nine pairs of pavement texture and friction data are analyzed in this article after three data sets are removed due to the bad data quality.

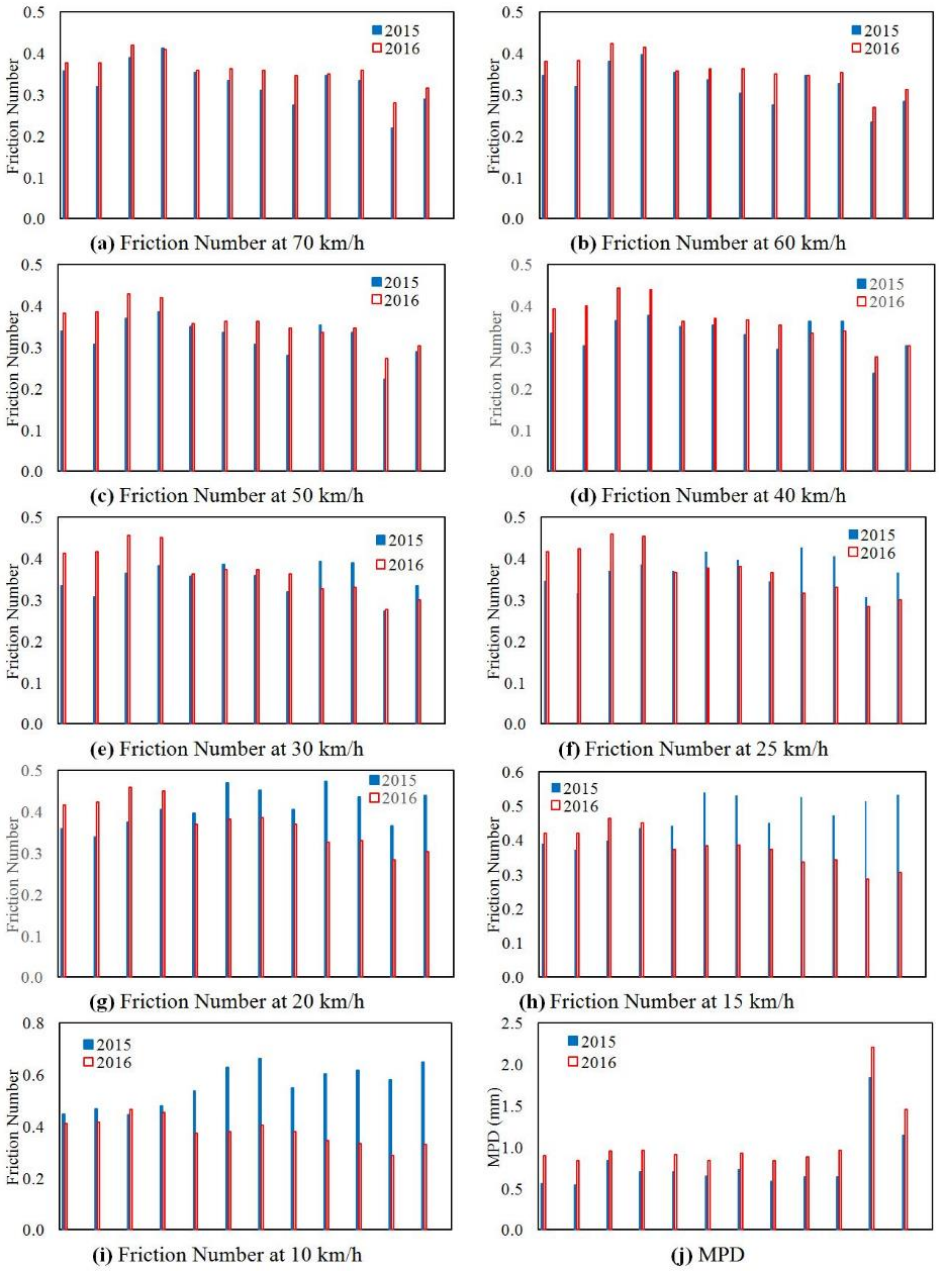

Figure 20 Average DFT Friction at Various Speeds and Summary of MPD

Note: The column labels in the figure are: Section 1, Transition 1, Section 2, Transition 2, … , Section 6, Transition 6 from left to right.

For preliminary analysis, MPD for each 3D measurement is calculated, while pavement DFT friction numbers at various testing speeds from 10 km/h to 70 km/h are produced. The average DFT friction numbers at speeds from 10 km/h to 70 km/h and the average MPD for each SPS-10 section and transition are plotted in Figure 20. It is

illustrated that the average friction numbers at speeds over 40 km/h show an increase tendency between the two data collection events (Figures 20(a) through 20(d)), whereas the average friction numbers at speeds lower than 20 km/h exhibit a decrease tendency for most of the locations (Figures 20(g) to 20(i)). For example, the average friction numbers at 60 km/h for Sections 1 through 6 are 0.35, 0.38, 0.35, 0.30, 0.35, and 0.23 for the first data collection in 2015, and 0.38, 0.42, 0.36, 0.36, 0.34 and 0.27 for the second collection in 2016. The average friction numbers at 10 km/h for Sections 1 through 6 are 0.45, 0.45, 0.54, 0.66, 0.60, and 0.58 in 2015, while 0.41, 0.47, 0.37, 0.41, 0.35 and 0.29 in 2016. At speeds from 20 km/h to 30 km/h (Figures 20(e) to 20(g)), no consistent tendency is observed on these sections. On the other hand, the average MPD values for each of the six SPS-10 section and transition section display an increasing tendency, as shown in Figure 20(j). The average MPD for Sections 1 through 6 are 0.56 mm, 0.84 mm, 0.71 mm, 0.73 mm, 0.64 mm, and 1.84 mm in 2015, and 0.90 mm, 0.95 mm, 0.91 mm, 0.93 mm, 0.88 mm and 2.21 mm in 2016.

Generally the evolution of skid resistance with an initial increase in friction coefficient occurs in the following months immediately after the laying of the road surface. Due to the applications of traffic polish, the bitumen film which masks the aggregate is gradually removed and the pavement friction number gradually increases. During the binder removal phase, more aggregate is exposed to the pavement surface. The binder removal period could range from 6 months to 2 years (54). Since 60 km/h is the standard testing speed to collect friction number (52), it is logical that the friction numbers have increased over the last 6 month as shown in Figure 20.b. In addition, “new” surface texture may be generated under potential “differential” traffic polishing (57), which probably results in the increase of the average MPD values during the last 6-month period.

On the other hand, Section 6 shows distinct higher average MPD values comparing to those on the other sections for both data collections (Figure 20(j)), while the average DFT friction numbers on Section 6 are relatively lower for testing speeds over 25 km/h (Figures 20(a) to 20(f)). The relatively lower insoluble residue value of the aggregate (Table 4.1) and the observed thick bitumen film after construction are the possible reasons for the lower skid resistance of Section 6. In addition, friction and MPD

data on Section 6 show opposite development tendency for both collection events at speeds lower than 20 km/h (Figures 20(g) to 20(j)). Since MPD fails to capture the differences and variations in friction performance both at high and low speeds, new texture parameters are needed to be developed to relate pavement texture with friction performance at macro- and micro-level.

4.4 3D Areal Texture Parameters

After a thorough literature review, there are five different categories of 3D areal parameters used in various areas: height parameters, volume parameters, hybrid parameters, spatial parameters, and feature parameters, all of which are calculated and used to relate pavement texture characteristics to friction performance in this study. The first four categories of parameters are generally classified as field parameters which are calculated using all the data point measured in a 3D surface. The last category is calculated based upon the features which play specific role in a particular function on a 3D image. For each category, several different texture parameters are used for various purposes. The definitions of the 3D areal parameters and their calculations for each category are provided in the following sections.

4.4.1 Height Parameters

The arithmetic mean height (Sa), the root mean square height (Sq), the skewness (Ssk), the Kurtosis (Sku), the maximum height of the surface (Sp, Sv, and Sz), and the traditional MPD are typical height texture parameters. The definitions of Sa, Sq, Ssk, and Sku are shown in Equations 4.1 to 4.4 individually:

$$S_a = 1/A \times \text{Interp2d}[z(x,y)] \quad (4.1)$$

$$S_q = \text{SQRT}\{1/A \times \text{Interp2d}[z^2(x,y)]\} \quad (4.2)$$

$$S_{sk} = 1/(S_q^3 \times A) \times \text{Interp2d}[z^3(x,y)] \quad (4.3)$$

$$Sk_u = 1/(S_q^4 \times A) \times \text{Interp2d}[z^4(x,y)] \quad (4.4)$$

Where Interp2d represents the double integration process; SQRT returns the square root of a number; the z(x,y) is the height of pixel in mm at location (x,y) within the 3D image (66).

Sp is the maximum peak height, Sv is the maximum pit height, and Sz is the maximum height of the surface (66). The calculation of MPD is defined in ASTM E1845-15 (67), which only considers the average height of the two highest peaks of two 50 mm

profile segments. Sa is generally used to capture the roughness variation of road surfaces under traffic wear in laboratory (56). Sa and Sq are insensitive in differentiating peaks, valleys and the spacing of the various texture features, thus pavement surfaces with same Sa or Sq may function quite differently (69).

4.4.2 Volume Parameters

The volume parameters, including the void volume (Vv), the material volume (Vm), the peak material volume (Vmp), the core material volume (Vmc), the core void volume (Vvc) and the dales void volume (Vvv), are function related parameters (66 and 69). The material ratio (mr), defined in Figure 21(a), is the ratio in percentage of the length of bearing surface at any specified depth in a profile (69). mr simulates surface wear of a 3D pavement surface which provides a bearing surface for vehicle tires. As the cutting plane moves down from the highest peak to the lowest valley of a profile, mr will increase along with the bearing surface and range up to 100%. The areal material ratio curve (the dashed line as shown in Figure 21(b)) is the cumulative curve of mr from the highest peak to the lowest valley (69).

Vv (Vm) for a material ratio mr is calculated by integrating the volume enclosed above (below) the 3D texture image and below (above) the horizontal cutting plane at the height corresponding to mr (66). Vvc (Vmc) is defined as the difference between two void (material) volume values calculated at different heights corresponding to mr1 and mr2, while Vvv (Vmp) is defined as the void (material) volume calculated at the height corresponding to mr2 (mr1):

$$V_{vc}=V_v(mr1)- V_v(mr2) \quad (4.5)$$

$$V_{mc}=V_m(mr2)- V_m(mr1) \quad (4.6)$$

$$V_{vv}=V_v(mr2) \quad (4.7)$$

$$V_{mp}=V_m(mr1) \quad (4.8)$$

Where mr1 = 10%, mr2 = 80%, and the unit of volume parameters is mm3/mm2 herein (66). In Figure 21(b), Vvc (Vmc) is the area enclosed above (below) the areal material ratio curve and between the heights corresponding to mr1 and mr2, and Vvv (Vmp) is the area enclosed above (below) the areal material ratio curve and between the height corresponding to mr2 (mr1). The volume parameters can characterize wear and rolling properties during a running-in procedure (70 and 71). Vmc is useful to

understand how much material is available for load support once the top levels of a surfaces are worn away (69).

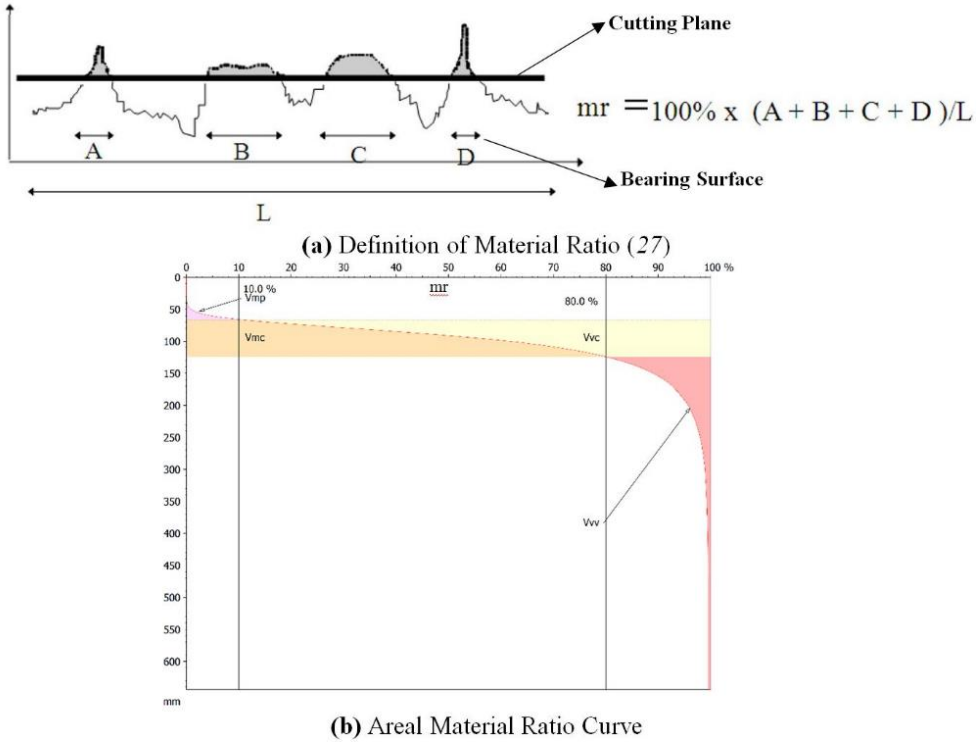

Figure 21 Calculation of Volume Parameters

4.4.3 Hybrid Parameters

The hybrid parameters are useful to consider both the height and spacing information of a 3D image simultaneously to evaluate texture characteristic (60). The root mean square gradient (Sdq) and developed interfacial area ratio (Sdr) are defined in Equation 4.9 and Equation 4.10 and considered herein to differentiate the surface with similar degree of roughness (66 and 69). Sdq and Sdr are affected both by texture amplitude and spacing: a surface with same roughness and wider spaced texture may induce a lower value of Sdq or Sdr (69).

$$S_{dq} = SQRT\{1/A \times Interp2d[Deriv2d(z,x) + Deriv2d(z,y)]\} \quad (4.9)$$

$$S_{dr} = (TSA-CSA)/CSA \quad (4.10)$$

Where Interp2d is the double integration and Deriv2d is the second derivative function; TSA is the texture surface area and CSA is the cross sectional area.

4.4.4 Spatial Parameters

The calculation of spatial parameters involves the understanding of the autocorrelation function (ACF) which evaluates the correlation of the original surface and the duplicated surface with a relatively shift (Dx, Dy) (66 and 68). The autocorrelation length (Sal) defines the distance over the surface such that the new location will have minimal correlation with the original location, and the texture aspect ratio (Str) is the division of the Sal and the length of slowest decay ACF in any direction (69). The texture direction (Std), with values between 0º and 180º, is also included to identify the angular direction of the dominant lay comprising a surface (68 and 69). Str can be applied to evaluate surface texture isotropy, and Sal may find application related to the interaction of electromagnetic radiation with the surface and also tribological characteristics such as friction and wear (68 and 69).

4.4.5 Feature Parameters

The feature parameters herein consider the peak density (Spd), the peak curvature (Spc), and the significant height (S5p, S5v, and S10z). A surface point higher than its surrounding area is called a peak, and the significant peaks on a surface are segmented by inverting the surface and applying the watershed segmentation algorithm and the pruning of the change tree by a specified pruning factor (66). Spd and Spc are defined in Equation 4 with unites of 1/mm2 and 1/mm respectively (66 and 68). S5p (S5v) is the arithmetic mean height of the five highest (lowest) significant peaks (pits), and S10z is simply the sum of S5p and S5v with unit of mm (66).

Spd can be used in applications where contact is involved along with other parameters, and the peak density can be used to quantify aggregate micro-texture with respect to wear in laboratory (57 and 66). Spc is useful in predicting the degree of elastic and plastic deformation of a surface under different loading conditions and thus may be used in predicting friction, wear and real area of contact for thermal/electrical applications (69). The curvature of a profile was able to quantify aggregate micro-texture with respect to the surface friction under wear condition in laboratory (57).

$$S_{pd} = (\text{Number of Peaks})/(\text{Area}) \quad (4.11)$$

$$S_{pc} = 1/N \times \text{Interp2d}_{\text{Peak-Area}}\{[\text{Deriv2d}(z,x) + \text{Deriv2d}(z,y)]\} \quad (4.12)$$

4.5 Selection of 3D Texture Parameters

4.5.1 Correlation Analysis

Considering all five categories of 3D areal parameters aforementioned, there are twenty-four different parameters available to represent the 3D texture characteristics of a pavement surface. The calculation of those parameters are calculated via the Mountains® software. The correlation analysis is conducted within each category and among different categories to remove the parameters who exhibit strong correlations and remove their potential multicollinearity for regressional friction model development. Correlation coefficient of 0 means that there is no correlation, -1 denotes a perfect negative correlation, while +1 suggests a perfect positive correlation between the two variables. A correlation greater than 0.8 is generally described as strong, whereas a correlation less than 0.5 is generally described as weak (72).

4.5.2 Correlation within Each Category

The correlation coefficients within each category are summarized in Tables 4.2 to 4.4.

- Based on Table 4.2, Sq and Ssk are kept to represent as the height parameters since their correlation coefficients with other parameters are less than 0.5. The traditional texture indicator MPD is excluded herein because it is highly correlated with many height parameters such as Sq, Sp, Sv, Sz, and Sa.
- Based on Table 4.3, only Vmc is kept as the volume parameter, and Sdq is selected as the hybrid parameter to evaluate the friction performance between the vehicle tire and the pavement surface.
- Based on Table 4.4, Sal and Str are selected as the spatial parameters while Spd, Spc and S5v are selected as feature parameters due to their lower correlation coefficients with other parameters.

In summary, after the correlation analysis within each texture parameter category, only Sq, Ssk, Vmc, Sdq, Sal, Str, Spd, Spc and S5v are determined as the potential 3D areal parameters, which are not highly correlated within each category, for the development of relationship between pavement texture and friction performance.

4.5.3 Correlation among Categories

Subsequently, correlation analysis among different categories is performed for the previously identified 3D parameters within each category, since correlations may be strong among the parameters within different categories. As shown in Table 4.5, Sq, Sdq, Str, Spc, and S5v are excluded because their correlation coefficients with other parameters are larger than 0.5. Correspondingly, Ssk, Vmc, Sal and Spd, which represents the height, volume, spatial and feature attributes of a 3D surface respectively, are selected as the final list of the 3D areal parameters for friction model development. The statistics of the selected 3D areal parameters on each SPS-10 section and transition are plotted in Figure 22 to evaluate the variations of these texture indicators between these two data collection events:

- Vmc and Spd demonstrate decreasing tendency with traffic polish for most locations (Figures 22(b) and 22(c)), while Ssk and Sal exhibit inconsistent tendency (Figures 22(a) and 22(d)).
- As can be seen in Figure 22(c) and Figure 20(i), the development of Spd corresponds well to the variation tendency of DFT friction number at the speed of 10 km/h.
- On the other hand, because Vmc represents the part of the surface material which does not interact with another surface in contact (66), the smaller the Vmc value, the more surface materials are involved in the contact process with vehicle tires. Therefore, it is observed from Figure 22(b), and Figures 20(a) and 20(b) that the development of Vmc corresponds well to the variation tendency of friction number at speeds over 60 km/h for all the sections.

Table 4.2 Correlation Analyses of 3D Height Texture Parameters

Parameter	**Sq**	**Ssk**	Sku	Sp	Sv	Sz	Sa	MPD
Sq	1.0	-0.2	0.3	0.9	0.9	1.0	1.0	0.9
Ssk	-0.2	1.0	-1.0	-0.3	-0.2	-0.1	-0.1	-0.2
Sku	0.3	-1.0	1.0	0.4	0.3	0.2	0.2	0.3
Sp	0.9	-0.3	0.4	1.0	1.0	0.9	0.9	0.9
Sv	0.9	-0.2	0.3	1.0	1.0	0.9	0.9	0.9
Sz	1.0	-0.1	0.2	0.9	0.9	1.0	1.0	0.9
Sa	1.0	-0.1	0.2	0.9	0.9	1.0	1.0	0.9
MPD	0.9	-0.2	0.3	0.9	0.9	0.9	0.9	1.0

Table 4.3 Correlation Analyses of 3D Volume and Hybrid Texture Parameters

Parameter	Vm	Vv	Vmp	**Vmc**	Vvc	Vvv	**Sdq**	Sdr
Vm	1.0	0.7	1.0	0.7	0.7	0.6	-	-
Vv	0.7	1.0	0.7	1.0	1.0	1.0	-	-
Vmp	1.0	0.7	1.0	0.7	0.7	0.6	-	-
Vmc	0.7	1.0	0.7	1.0	1.0	0.9	-	-
Vvc	0.7	1.0	0.7	1.0	1.0	0.9	-	-
Vvv	0.6	1.0	0.6	0.9	0.9	1.0	-	-
Sdq	-	-	-	-	-	-	1.0	0.8
Sdr	-	-	-	-	-	-	0.8	1.0

Table 4.4 Correlation Analyses of 3D Spatial and Feature Texture Parameters

Parameter	**Sal**	**Str**	Std	**Spd**	**Spc**	S10z	S5p	**S5v**
Sal	1.0	-0.3	-0.1	-	-	-	-	-
Str	-0.3	1.0	0.5	-	-	-	-	-
Std	-0.1	0.5	1.0	-	-	-	-	-
Spd	-	-	-	1.0	-0.3	-0.3	-0.3	-0.3
Spc	-	-	-	-0.3	1.0	0.9	0.8	0.9
S10z	-	-	-	-0.3	0.9	1.0	0.9	0.9
S5p	-	-	-	-0.3	0.8	0.9	1.0	0.6
S5v	-	-	-	-0.3	0.9	0.9	0.6	1.0

Table 4.5 Correlation Analyses Among All Categories of 3D Texture Parameters

Parameter	Sq	**Ssk**	**Vmc**	Sdq	**Sal**	Str	**Spd**	Spc	S5v
Sq	1.0	-0.2	1.0	0.7	-0.1	0.6	-0.3	0.8	0.8
Ssk	-0.2	1.0	0.0	0.2	0.2	0.2	0.4	0.1	-0.0
Vmc	1.0	0.0	1.0	0.7	-0.1	0.6	-0.3	0.9	0.9
Sdq	0.7	0.2	0.7	1.0	-0.0	0.4	-0.1	0.8	0.7
Sal	-0.0	0.2	-0.1	-0.0	1.0	-0.3	-0.1	-0.1	-0.1
Str	0.6	0.2	0.6	0.4	-0.3	1.0	-0.1	0.5	0.5
Spd	-0.3	0.4	-0.3	-0.1	-0.1	-0.1	1.0	-0.3	-0.3
Spc	0.8	0.1	0.9	0.8	-0.1	0.5	-0.3	1.0	0.9
S5v	0.8	-0.0	0.9	0.7	-0.1	0.5	-0.3	0.9	1.0

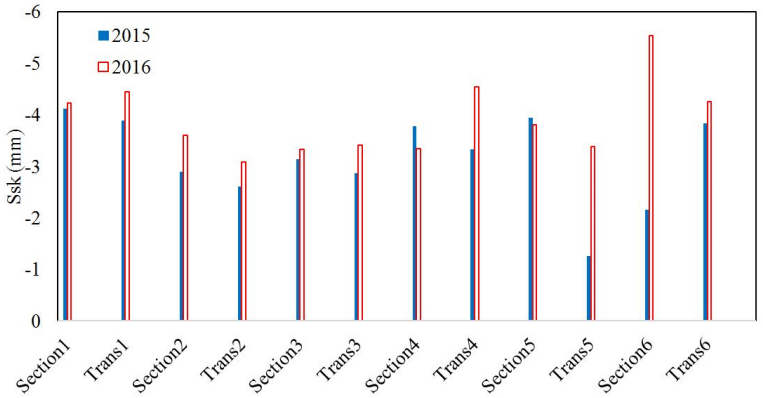

(a) Skewness, Ssk

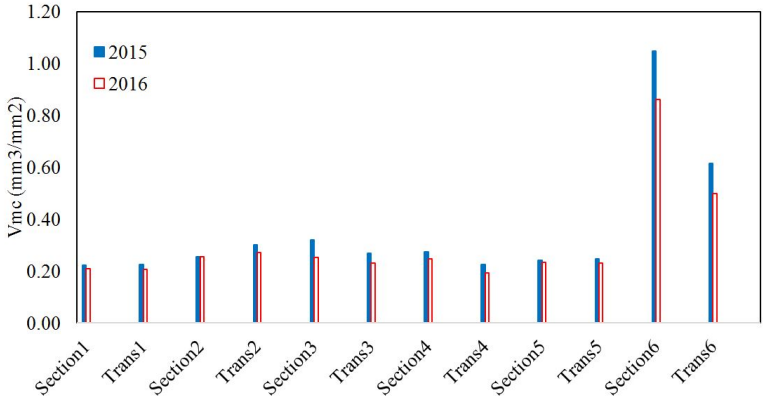

(b) Core Material Volume, Vmc

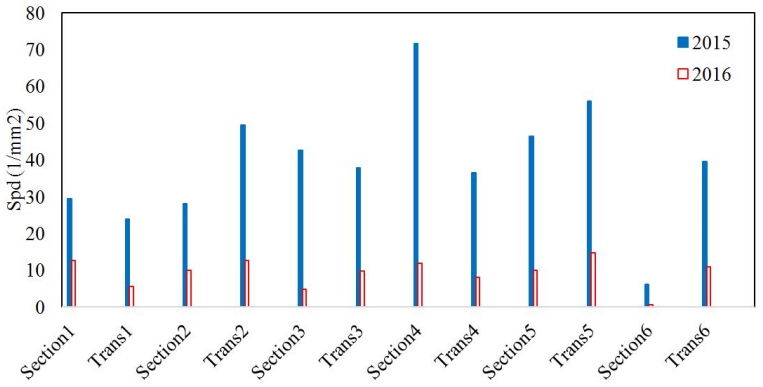

(c) Peak Density, Spd

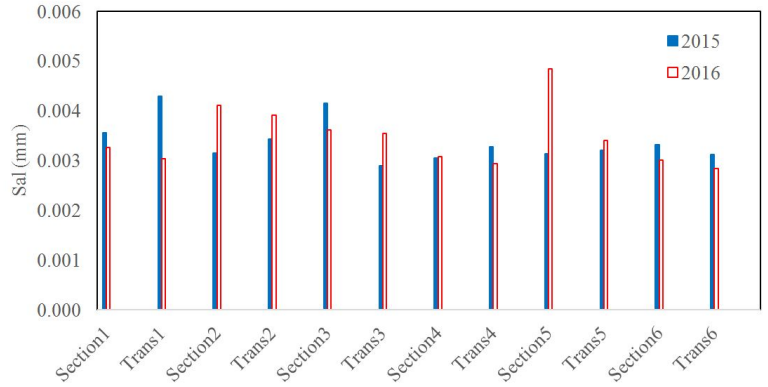

(d)Autocorrelation Length, Sal

Figure 22 Comparisons of Selected 3D Pavement Texture Parameters

4.6 Friction Prediction Model based on selected 3D Areal Texture Parameters

4.6.1 Model Development

The sixty-nine sets of DFT friction numbers at different speeds along with the selected 3D areal texture parameters, Ssk, Vmc, Sal and Spd, are prepared for model development. Every other data sets are used to develop the friction prediction model at different speeds, while the remaining data sets are reserved for model validation. Multivariate linear regression analysis is conducted to identify the significant confidence level of the selected 3D areal texture parameters on friction number at different speeds, and the results are summarized in Table 4.6:

- Vmc and Spd show consistently significant influence on friction numbers for testing speeds over 25 km/h and less than 20 km/h, individually.
- Ssk is identified as a significant parameter for DFT friction tested at speed of 10 km/h only.
- Sal is not a significant factor on friction at any speeds among these selected four parameters.

Table 4.6 Significance of Selected 3D Texture Parameters on DFT Friction at Different Speeds

3D Parameter	DFT70	DFT60	DFT50	DFT40	DFT30	DFT25	DFT20	DFT15	DFT10
Ssk	-	-	-	-	-	-	-	*	*
Vmc	**	**	**	**	**	*	-	-	*
Sal	-	-	-	-	-	-	-	-	-
Spd	-	-	-	-	-	-	*	**	***

Note: DFTxx means the DFT friction number collected at xx km/h; Significance codes: '***' 0.001, '**' 0.01, '*' 0.05, '-' 0.05. For example '*' indicates the P-value is less than 0.05 and the parameter is significant to the friction number; '-' means the P-value is larger than 0.05 and the parameter is not significant to the friction number.

Subsequently, friction prediction models are developed based on only the significant 3D areal parameters at different speeds. The estimated regression coefficients and P-values of friction prediction models are summarized in Table 4.7. All the P-values for the 3D areal texture parameter herein are smaller than 0.05 in the proposed model, indicating their significance to pavement friction. Therefore, the friction

number at different speeds are valid and can be calculated based on the selected 3D areal parameters as Equation 4.5:

$$\text{Friction Number} = a + \text{Sum}\,(T_i \times b_i) \quad (4.5)$$

Where a is the estimated coefficient for intercept, T_i represents the Vmc, Ssk and Spd of a 3D pavement surface, and b_i is the estimated coefficient for the corresponding 3D areal parameter at different speeds.

Table 4.7 Statistic Results of Friction Prediction Models based on Selected 3D Areal Texture Parameters

Friction #	Variable	Coefficient	P-value	R^2	SSE
70 km/h	Intercept	0.395	6.36E-26	0.58	0.031
	Vmc	-0.138	8.07E-05		
60 km/h	Intercept	0.394	7.58E-26	0.57	0.034
	Vmc	-0.144	4.54E-05		
50 km/h	Intercept	0.391	4.38E-26	0.54	0.038
	Vmc	-0.136	7.63E-05		
40 km/h	Intercept	0.394	3.83E-26	0.48	0.044
	Vmc	-0.127	0.00018		
30 km/h	Intercept	0.399	2.74E-25	0.37	0.057
	Vmc	-0.110	0.001804		
25 km/h	Intercept	0.405	1.16E-24	0.29	0.066
	Vmc	-0.091	0.012268		
20 km/h	Intercept	0.362	2.81E-23	0.33	0.089
	Spd	0.001	0.003921		
15 km/h	Intercept	0.368	5.68E-21	0.38	0.131
	Spd	0.002	8.28E-05		
10 km/h	Intercept	0.414	1.63E-07	0.54	0.209
	Ssk	0.027	0.043722		
	Vmc	0.181	0.002568		
	Spd	0.004	3.21E-06		

Table 4.8 Statistic Results of Friction Prediction Models based on MPD

Friction #	Variable	Coefficient	P-value	R^2	SSE
70 km/h	Intercept	0.401	2.44E-20	0.30	0.051
	MPD	-0.055	5.52E-03		
60 km/h	Intercept	0.399	4.80E-20	0.29	0.055
	MPD	-0.056	5.15E-03		
50 km/h	Intercept	0.397	1.91E-20	0.26	0.060
	MPD	-0.054	5.76E-03		
40 km/h	Intercept	0.399	1.09E-20	0.25	0.063
	MPD	-0.050	0.00832		

Friction #	Variable	Coefficient	P-value	R^2	SSE
30 km/h	Intercept	0.407	1.06E-20	0.26	0.067
	MPD	-0.048	0.01288		
25 km/h	Intercept	0.420	5.22E-21	0.26	0.069
	MPD	-0.048	0.01302		
20 km/h	Intercept	0.441	5.12E-20	0.21	0.097
	MPD	-0.048	0.02860		
15 km/h	Intercept	0.473	1.29E-16	0.10	0.192
	MPD	-0.048	0.10751		
10 km/h	Intercept	0.531	6.87E-13	0.16	0.373
	MPD	-0.061	0.18092		

4.6.2 Model Verification

Based on Equation 4.5, the predicted friction numbers of the validation data sets are calculated and compared with the actual friction numbers to validate the proposed models. The validation results of the developed friction prediction model at different speeds are also summarized in Table 4.8. The R-squared values are 0.54 to 0.58 between the predicted and the actual DFT friction numbers at speeds from 10 km/h to 70 km/h, respectively. Generally speaking, the friction prediction models at higher testing speeds have better performance than those at lower speeds. The sum of squared error (SSE) for the proposed models at speed 70 km/h to 10 km/h increases from 0.031 to 0.209. Example of the actual and the predicted friction numbers at high and low speeds are compared in Figures 23(a) and 23(b).

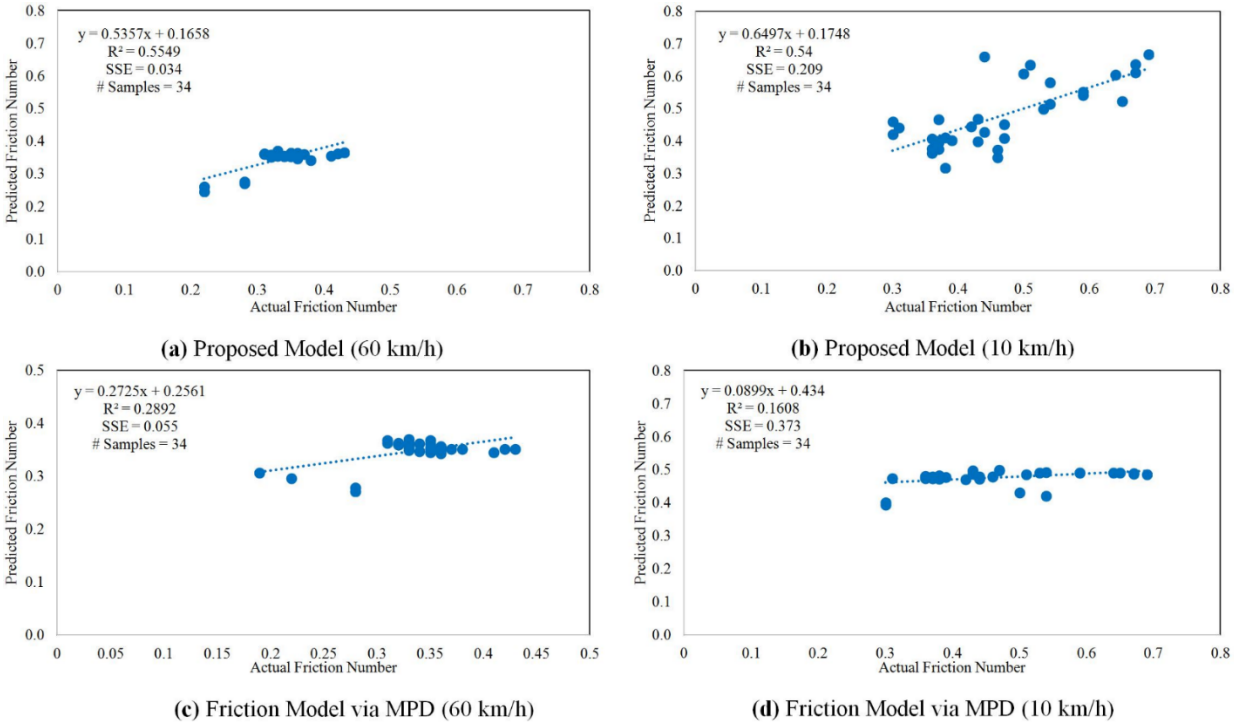

Figure 23 Model Validation and Comparisons

To demonstrate the advantages of the proposed parameters, linear regression friction prediction models at different testing speeds are also developed considering MPD as the influencing texture parameter. The estimated regression coefficients and P-values are also provided in Table 4.8. The P-values for the MPD based models are smaller than 0.05 for testing speeds over 20 km/h, indicating the significance of MPD to pavement friction at high speed. However, the P-values are greater than 0.05 for models at the testing speeds of 15 km/h and 10 km/h, indicating the insignificance of MPD to pavement friction at low speed. The R-squared values of the MPD based models range from 0.1 to 0.3 between the predicted and actual DFT friction numbers, which are much lower than those for the proposed models based on the 3D texture indicators. In addition, the sum of squared errors of prediction (SSE) in the MPD based model are consistently higher than those in the models from this paper, proving that the DFT friction models based on the selected 3D areal texture parameters are more robust. Examples of the actual and the predicted friction numbers at high and low speeds are compared in Figures 23(c) and 23(d).

Based on Tables 4.6, 4.7 and 4.8, Vmc is the only significant parameter on friction number for the models at speeds over 20 km/h, whereas the Spd is the only

significant parameter on friction number for the models at speeds 20 km/h and 15 km/h. Even though there are three significant parameters in the model at 10 km/h, Spd is the dominate parameter over the other two based on their P-values. Therefore, it can be concluded that Vmc and Spd are the 3D areal parameters corresponding to macro- and micro-texture for friction prediction at high (over 40 km/h) and low speeds (lower than 15 km/h).

4.7 Conclusions

The objective of this work is to identify suitable pavement texture parameters under 3D to characterize pavement surface texture and friction performance. The LS-40 Portable 3D Surface Analyzer and the Dynamic Friction Tester with necessary software tools are used to perform pavement texture and friction data collection and subsequent calculation of 3D areal parameters and friction numbers at different testing speeds. The 3D surface range data with the resolution of 0.01 mm and 0.05 mm in vertical and lateral direction are collected on the newly constructed LTPP SPS-10 site in Oklahoma with 6 WMA sections. Twenty-four 3D areal texture parameters from five categories, including height parameter, volume parameters, hybrid parameters, spatial parameters and feature parameters, are explored in the study and calculated for each 3D surface data collection to comprehensively evaluate the pavement surface texture characteristics.

Correlation analysis is performed within each texture indicator category and among the categories to select the most relevant and representative 3D areal parameters for friction model development. The results show that Vmc (a volume parameter) and Spd (a feature parameter) can relate the pavement texture at macro- and micro-level for friction in wet conditions at high and low speeds respectively. Multivariate linear regression pavement friction prediction models are developed based on the selected 3D areal texture parameters at different speeds. The validation results demonstrate that the developed friction prediction models produce fairly accurate friction predictions. The selected 3D texture parameters provide better alternative to characterize texture attributes with respect to pavement friction performance, and have the potential to replace the existing contact-based friction measurement methodologies

which require consuming water and testing tires with non-contact high-resolution 3D laser-imaging based techniques.

It is also recognized that only sixty-nine pairs of data sets are collected in this study for the selection of 3D pavement texture parameters and the development of friction prediction models. More 3D data sets should be collected in the future to validate the applicability of the identified 3D texture parameters and the proposed friction prediction models. In addition, more 3D texture parameters should be explored to better capture the pavement texture and characterize friction simultaneously.

5. CONCLUSIONS

The 3D Ultra laser imaging technology has the capability to collect pavement surface texture data at full-lane coverage at 1 mm resolution in all three dimensions at the data collection speed up to 60MPH. This single-pass and complete lane coverage platform provides an ideal solution to evaluate pavement surface characteristics for safety analysis and many different data needs without interrupting traffic.

In this study, the 3D Ultra laser imaging technology with necessary software tools are utilized for data collection and subsequent surface characterization and safety evaluation and analysis. The first application of using 1mm 3D Ultra data sets is to predict and evaluate pavement surface hydroplaning risk. Considering the effects of flow path slope on vertical wheel load perpendicular to pavement surface and the resulting hydroplaning speed, the Gallaway and USF models are modified for improvements in this study. The sensitivity analysis shows that the hydroplaning speed is more sensitive to cross slope than longitudinal grade in the improved models. A 3D based volumetric measuring method is used to calculate the estimated MTD based on the full-lane 1mm 3D data. Subsequently, IMU data and 3D data are combined to model vehicle movements on cross slopes. Local rainfall intensity is obtained from NOAA precipitation database. By considering effects of cross slope and longitudinal grade on wheel load and flow path length, it is found that hydroplaning speed decreases with the increase of the longitudinal grade, but increases with the increase of the cross slope. The improved models predict lower hydroplaning speed than that from the original Gallaway and USF models. An important future work is to use a combined slope based on longitudinal grade and cross slop to demonstrate the validity and effectiveness of the improved models.

In addition, pavement macro-texture and friction data from six HFST sites that were installed on existing SMA, PCC, and HMA pavement surfaces are analyzed. 15 pairs of pavement macro-texture and friction data were collected with length ranging from 358 m to 1184 m considering the number of lanes and traffic directions of the sites. Total energy and the relative energy distributions are calculated for the decomposed macro-texture profiles from wavelet transform, and the relationship between the energy indicators and pavement friction performance is studied. The energy distributions for

macro-texture on the different pavement surfaces could vary significantly. On HFST sections, more than 50% of the energy is distributed within the 1st to the 4th decompositions levels (D1 to D4), with the wavelengths ranging from 0.97 mm to 7.72 mm. While for the other three pavement surface types, including SMA, PCC, and tradition HMA, more than 50% of the energy of macro-texture profiles is distributed within the 5th to the 7th decomposition levels (D5 to D7) with longer wavelengths ranging from 15.44 mm to 61.77 mm. Seven decomposition levels are considered in this section for macro-texture analysis. All the energy indicators for the seven levels show significant contributions to the pavement friction performance, which are used as the independent variables for friction model development. The energies at wavelengths from 0.97 mm to 3.86 mm contributes positively to pavement friction while those at wavelengths from 15.44 mm to 61.77 mm demonstrates negative impacts.

The third application is to identify suitable pavement texture parameters under 3D to characterize pavement surface texture and friction performance. The LS-40 Portable 3D Surface Analyzer and the Dynamic Friction Tester with necessary software tools are used to perform pavement texture and friction data collection and subsequent calculation of 3D areal parameters and friction numbers at different testing speeds. The 3D surface range data with the resolution of 0.01 mm and 0.05 mm in vertical and lateral direction are collected on the newly constructed LTPP SPS-10 site in Oklahoma with 6 WMA sections. Twenty-four 3D areal texture parameters from five categories, including height parameter, volume parameters, hybrid parameters, spatial parameters and feature parameters, are explored in the study and calculated for each 3D surface data collection to comprehensively evaluate the pavement surface texture characteristics. Correlation analysis is performed within each texture indicator category and among the categories to select the most relevant and representative 3D areal parameters for friction model development. The results show that Vmc (a volume parameter) and Spd (a feature parameter) can relate the pavement texture at macro- and micro-level for friction in wet conditions at high and low speeds respectively. Multivariate linear regression pavement friction prediction models are developed based on the selected 3D areal texture parameters at different speeds. The validation results demonstrate that the developed friction prediction models produce fairly accurate

friction predictions. The selected 3D texture parameters provide better alternative to characterize texture attributes with respect to pavement friction performance, and have the potential to replace the existing contact-based friction measurement methodologies which require consuming water and testing tires with non-contact high-resolution 3D laser-imaging based techniques.

This study with field pavement applications has shown that the 1mm 3D Ultra technology is promising in real-time pavement surface characterization and evaluation for both pavement and safety management at network and project level surveys. It is anticipated that more tests and refinements are to be performed to validate the new emerging 3D laser imaging technology as a single-pass and complete lane-coverage platform for multiple safety and pavement evaluation purposes. One such refinement is to increase the resolution of the 3D sensors to sub-mm. In addition, the long-term monitoring of the HFTS and WMA sites in multiple states is highly recommended due to the need to determine multi-year performance of the HFTS applications in terms of region, pavement condition, materials used, geometric properties, and other factors. The recommended long-term study would provide much needed data for both design and construction of HFTS for its widespread adoption.

REFERENCES

[1] Kumar, S.Santosh, Anupam, Kumar, and FWA, T.F. Analyzing effect of tire groove patterns on hydroplaning speed, *Journal of the Eastern Asia Society for Transportation Studies*, Vol. 8. 2009

[2] Khedr, Safwan A. and Breakah, Tamer M. Rutting parameters for asphalt concrete for different aggregate structures, *International Journal of Pavement Engineering*, Volume 12, Issue 1, pp 13-23, 2011.

[3] M.ISH, Rohit Goyal. Design and Analysis of Interceptor Drains—Effect of Parameters, *ISH Journal of Hydraulic Engineering*, Volume 9, Issue 1, pp 61-71, 2003.

[4] Horne, W.B., and R.C. Dreher.1963 Phenomena of Pneumatic Tire Hydroplaning, NASA TN D-2-56, NASA Langley Research center, NASA, Hampton, VA.

[5] Chesterton, John, Nancekivell, Noel, and Tunnicliffe, Noel. The use of the Gallaway Formula for Aquaplaning Evaluation in New Zealand, *Transit New Zealand and New Zealand Institute of Highway Technology (NZIHT) 8thAnnual Conference*, 2006.

[6] Russam, K. and Ross, N.F. The Depth of Rain Water on Road Surfaces. Road Research Laboratory, *Ministry of Transport Report* No. LR 236, pp25, 1968.

[7] Gallaway, B. M., et al. Pavement and Geometric Design Criteria for Minimizing Hydroplaning," Federal Highway Administration, Report No. FHWA-RD-79-31, 1979.

[8] Huebner. R.S., et al. PAVDRN Computer Model for Predicting Water Film Thickness and Potential or Hydroplaning on New and Reconditioned Pavements, *Transport Research Record* 1599 pp. 128-131, 1996.

[9] Gunaratne, M., Lu, Q., Yang, J. Hydroplaning on Multi Lane Facilities, Report for Florida Department of Transportation, Report No. BDK84 977-14, 2012.

[10] Zhang, Zhongjie , Abu-Farsakh, Murad Y. and Tao, Mingjiang. Evaluation of trench backfills at highway cross-drains, *International Journal of Pavement Engineering*, Volume 6, Issue 2, pp77-87, 2005.

[11] Gallaway, B. M., and Rose, Gerry. The Effects of Rainfall Intensity, Pavement Cross Slope, Surface Texture, and Drainage Length on Pavement Water Depths, Texas Transportation Institute, Research Report No. 138-5, 1971.

[12] Ong, G.P. and Fwa, T.F. Wet-pavement hydroplaning risk and skid-resistance: Modeling, *ASCE Journal of Transportation Engineering,* Vol. 133, No. 10, 2007.

[13] Shafabakhsh G.A., Kashi E. "Effect of Aircraft Wheel Load and Configuration on Runway Damages", *Period. Polytech. Civil Eng.,* Vol. 59, No. 1, pp. 85-94, 2015.

[14] Wang, Kelvin C.P. Automated Survey of Pavement Distress based on 2D and 3D Laser Images, *Report for MBTC* DOT 3023, 2011.

[15] Luo, Wenting, Wang, Kelvin C. P., Li, Lin. Surface Drainage Evaluation for Rigid Pavements Using IMU and 1 mm 3D Texture Data, Transportation Research Record: *Journal of the Transportation Research Board*, Washington, D.C, Pavement Management 2014, Volume 3, pp 121–128, 2014.

[16] ASTM. Measuring Pavement Macro-texture Depth Using a Volumetric Technique", ASTM Standard Practice E 965 *Book of ASTM Standards, Volume 04.03* Philadelphia, P A. 2006.

[17] ASTM. Measuring Pavement Macro-texture Properties Using the Circular Track Meter", ASTM Standard Practice E 2157 *Book of ASTM Standards, Volume 04.03* Philadelphia, P A. 2006.

[18] ASTM. Measuring Pavement Texture Drainage Using an Outflow. ASTM Standard Practice E 2380 *Book of ASTM Standards, Volume 04.03* Philadelphia, P A, 2006.

[19] ASTM. Measuring Surface Frictional Properties Using the British Pendulum Tester, ASTM Standard Practice E 303 *Book of ASTM Standards, Volume 04.03* Philadelphia, P A, 2006.

[20] ASTM. Standard Practice for Calculating Pavement Macro-texture Mean Profile Depth, ASTM Standard Practice E 1845-01 *Book of ASTM Standards, Volume 04.03* Philadelphia, P A, 2005.

[21] Wang, Kelvin C.P. "Safety Evaluation of Pavement Surface Characteristics with 1mm 3D Laser Imaging", RiP Project 37465, Nov 7 2014.

[22] Wang, Kelvin C.P., Li, Lin. Potential Measurement of Pavement Surface Texture based on Three-Dimensional (3D) Image Data, *Transportation Research Board 91th Annual Meeting*, Washington, D.C. USA, 2011.

[23] Wang, Kelvin C. P., Luo, Wenting, and Li, Joshua Q. Hydroplaning Risk Evaluation of Highway Pavements based on IMU and 1 mm 3D Texture Data, *T&DI Congress 2014: Planes Trains, and Automobiles*, Advanced Technologies for Transportation Application, pp. 511-522, 2014.

[24] Mekemson et al. Method and Apparatus for Pavement Cross-slope Measurement, Patent Application Publication, Pub. No.: US 2002/0013644 A1, 2002.

[25] NOAA's National Water Service. Hydrometeorological Design Studies Center, "Precipitation Frequency Data Server (PFDS)": http://dipper.nws.noaa.gov/hdsc/pfds/, Accessed on July, 2014.

[26] Shah, Yogesh U., Jain, S.S., and Parida, Manoranjan. Evaluation of prioritization methods for effective pavement maintenance of urban roads, International Journal of Pavement Engineering, Volume 15, Issue 3, pp 238-250, 2014.

[27] Hall J.W. et al. NCHRP Web Document 108: Guide for Pavement Friction. Transportation Research Board, National Research Council, Washington, D.C., 2009.

[28] Najafi S. et al. Linking Roadway Crashes and Tire-Pavement Friction: A Case Study. International Journal of Pavement Engineering, DOI: 10.1080/10298436.2015.1039005. 2015.

[29] Henry J.J. NCHRP Synthesis 291: Evaluation of Pavement Friction Characteristics. Transportation Research Board, National Research Council, Washington, D.C. 2000.

[30] Ergun M., Iyinam S., and Iyinam A.F. Prediction of Road Surface Friction Coefficient Using Only Macro- and Microtexture Measurements. Journal of Transportation Engineering, 131(4), 311-319. 2005.

[31] Ahammed M.A. and Tighe S.L. Concrete Pavement Surface Textures and Multivariables Frictional Performance Analysis: a North American Case Study. Canadian Journal of Civil Engineering, Vol. 35, No. 7, 727-738. 2008.

[32] Ahammed M.A. and Tighe S.L. Asphalt Pavements Surface Texture and Skid Resistance – Exploring the Reality. Canadian Journal of Civil Engineering, Vol. 39, 1-9. 2012.

[33] Rezaei A. and Masad E. Experimental-based Model for Predicting the Skid Resistance of Asphalt Pavements. International Journal of Pavement Engineering, Vol. 14, No. 1, 24-35. 2013.

[34] Ueckermann et al. A Contribution to Non-contact Skid Resistance Measurement. International Journal of Pavement Engineering, Vol. 16, No. 7, 646-659. 2015.

[35] Ueckermann et al. Calculation of Skid Resistance from Texture Measurements. Journal of Traffic and Transportation Engineering, Vol. 2, No. 1, 3-16. 2015.

[36] Rado Z. and Kane M. An Initial Attempt to Develop an Empirical Relation between Texture and Pavement Friction Using the HHT Approach. Wear, Vol. 309, 233-236. 2014.

[37] Kane M., Rado Z. and Timmons A. Exploring the Texture-Friction Relationship: from Texture Empirical Decomposition to Pavement Friction. International Journal of Pavement Engineering, 16:10, 919-918, DOI:10.1080/10298436.2014.972956. 2015.

[38] Izeppi E., Flintsch G. and McGhee K. Field Performance of High Friction Surfaces. Publication FHWA/VTRC 10-CR6. FHWA, U.S. Department of Transportation. 2010. Available from http://www.virginiadot.org/vtrc/main/online_reports/pdf/10-cr6.pdf. [Accessed 15 Mar. 2016].

[39] Misiti M., Oppenheim G. and Poggi J. Wavelet Toolbox for Use with MATLAB: User's Guide. The MathWorks, Inc., Natick, MA. 2000.

[40] Hester D. and Gonzàlez A. A Wavelet-based Damage Detection Algorithm based on Bridge Acceleration Response to A Vehicle. Mechanical Systems and Signal Processing, 28, 145-166. 2012.

[41] Abbasnia R. and Farsaei A. Corrosion Detection of Reinforced Concrete Beams with Wavelet Analysis. International Journal of Civil Engineering, Transaction A: Civil Engineering, Vol. 11, No. 3, 160-169. 2013.

[42] Wang Kelvin C.P. Li Q. and Gong W., Wavelet-Based Pavement Distress Image Edge Detection with à Trous Algorithm. In Transportation Research Record: Journal of the Transportation Research Board, No. 2024, Transportation Research Board of the National Academies, Washington, D.C., 73–81. 2007.

[43] Wei L. et al. Wavelet Analysis and Interpretation of Road Roughness. Journal of Transportation Engineering. 131(2): 120-130. 2005.

[44] Alhasan A. White D.J. and Brabanterb K.D. Continuous Wavelet Analysis of Pavement Profiles. Automation in Construction, Vol. 63, 134-143. 2016.

[45] Hassan R. Two Applications of Wavelet Analysis for Project Level Pavement Management. International Journal of Sustainable Development and Planning, 10(2), 217-228. 2015.

[46] Zelelew H.M. et al. Pavement Macro-texture Analysis Using Wavelets. International Journal of Pavement Engineering, 14:8, 725-735, DOI: 10.1080/10298436.2012.705004. 2013.

[47] Zelelew H.M. et al. Wavelet-based Characterisation of Asphalt Pavement Surface Macro-texture. Road Materials and Pavement Design, 15:3, 622-641, DOI:10.1080/14680629.2014.908137. 2014.

[48] American Traffic Safety Services Association (ATSSA). Safety Opportunities in High Friction Surfacing. 2013. Available from http://www.dbiservices.com/sites/default/files/resources/ATSSA-HFST-LoRes.pdf. [Accessed 14 Mar. 2016].

[49] Merritt D. and Moravec M. An Update on HFST for Horizontal Curves. Proceeding of Pavement Evaluation 2014, Blacksburg, Virginia. 2014. Available from https://vtechworks.lib.vt.edu/bitstream/handle/10919/54619/Merritt_2.pdf?sequence=1&isAllowed=y [Accessed 14 Mar. 2016].

[50] ASTM Standard E1845-09. Standard Practice for Calculating Pavement Macro-texture Mean Profile Depth. ASTM International, West Conshohocken, PA, DOI: 10.1520/E1845-09. 2009.

[51] Papagiannakis, T., Zelelew, H. and Muhunthan, B. A wavelet interpretation of pavement-vehicle interaction. International Journal of Pavement Engineering, 8(3), 245–252. 2007.

[52] ASTM Standard E1911-09a. Standard Test Method for Measuring Paved Surface Frictional Properties Using the Dynamic Friction Tester. ASTM International, West Conshohocken, PA, DOI: 10.1520/E1911-09AE01, 2009.

[53] ASTM Standard E274/E274M-115. Standard Test Method for Skid Resistance of Paved Surfaces Using a Full-Scale Tire. ASTM International, West Conshohocken, PA, DOI: 10.1520/E0274_E0274M-15, 2015.

[54] Do M. et al. Pavement Polishing-Development of a Dedicated Laboratory Test and its Correlation with Road Results. Wear, Vol. 263, pp. 36-42, 2007.

[55] Flintsch G.W. et al. The Little Book of Tire Pavement Friction. Pavement Surface Properties Consortium, 2012. Available from https://secure.hosting.vt.edu/www.apps.vtti.vt.edu/1-pagers/CSTI_Flintsch/The%20Little%20Book%20of%20Tire%20Pavement%20Friction.pdf. [Accessed 1 May. 2016].

[56] Dunford A.M. et al. Three-Dimensional Characterization of Surface Texture for Road Stones Undergoing Simulated Traffic Wear. Wear, Vol. 292-293, pp. 188-196, 2012.

[57] Nataadmadja A.D. et al. Quantifying Aggregate Microtexture with Respect to Wear-Case of New Zealand Aggregates. Wear, Vol. 332-333, pp. 907-917, 2012.

[58] Villani M.M. et al. Application of Fractal Analysis for Measuring the Effects of Rubber Polishing on the Friction of Asphalt Concrete Mixtures. Wear, Vol. 320, pp. 179-188, 2014.

[59] Hartikainen L., Petry F. and Westermann S. Frequency-wise Correlation of the Power Spectral Density of Asphalt Surface Roughness and Tire Wet Friction. Wear, Vol. 317, pp. 111-119, 2014.

[60] Li L., Wang K.C.P., and Li Q.J. Geometric Texture Indicators for Safety on AC Pavements with 1 mm 3D Laser Texture Data. International Journal of Pavement Research and Technology, Vol. 9, pp. 49-62, 2016.

[61] Liu Q. and Shalaby A. Relating Concrete Pavement Noise and Friction to Three-Dimensional Texture Parameters. International Journal of Pavement Engineering, DOI: 10.1080/10298436.2015.1095897, 2015.

[62] Serigos P.A. The Contribution of Micro- and Macro-Texture to the Skid Resistance of Pavements. 2013. Available from http://www.ectri.org/YRS13/Documents/Presentations/Session5b-6a/YRS13_Session5b-6a_Serigos_TRB.pdf. [Accessed 12 May. 2016].

[63] Li S. et al. Pavement Surface Microtexture: Testing, Characterization and Frictional Interpretation. Available from http://www.astm.org/COMMIT/E17Presentations/5_PavementSurfaceMicrotexture.pdf. [Accessed 3 May. 2016].

[64] Kanafi M.M. et al. Macro- and Micro-Texture Evolution of Road Pavements and Correlation with Friction. International Journal of Pavement Engineering, Vol. 16, No. 2, pp. 168-179, DOI: 10.1080/10298436.2014.937715, 2015.

[65] Bitelli G. et al. Laser Scanning on Road Pavements: A New Approach for Characterizing Surface Texture. Sensors, Vol. 12, pp. 9110-9128, DOI: 10.3390/s120709110, 2012.

[66] Leach R. Characterisation of Areal Surface Texture. Springer-Verlag Berlin Heidelberg, DOI: 10.1007/978-3-642-36458-7, 2012.

[67] ASTM Standard E1845-15. Standard Practice for Calculating Pavement Macro-texture Mean Profile Depth. ASTM International. West Conshohocken, PA, DOI: 10.1520/E1845, 2015.

[68] Puccinelli J. et al. Long-Term Pavement Performance Warm Mix Asphalt Study. FHWA, VA. 2014.

[69] Michigan Metrology Surface Texture Parameters Glossary. Michigan Metrology, LLC, MI. 2014.

[70] Deltombe R., Kubiak K.J., Bigerelle M. How to Select the Most Relevant 3D Roughness Parameters of A Surface. Scanning, Vol. 36, No. 1, pp. 150-160, DOI: 10.1002/sca.21113, 2011.

[71] Adelle W. Quantitative Characterisation of Surface Finishes on Stainless Steel Sheet using 3D Surface Topography Analysis. 2006, Doctoral thesis, University of Huddersfield.

[72] Correlation Coefficient. MathBits.com. Available from http://mathbits.com/MathBits/TISection/Statistics2/correlation.htm. [Accessed 9 Jul. 2016].